ASSESSING THE STATE OF INITIAL POST-FIRE VEGETATION REGENERATION FOLLOWING A SEVERE MONTANE WILDLAND FIRE

JESSE ASPINALL
Bachelor of Science, University of Lethbridge, 2019

A thesis submitted
in partial fulfilment of the requirements for the degree of

MASTER OF SCIENCE

in

GEOGRAPHY

Department of Geography and Environment
University of Lethbridge
LETHBRIDGE, ALBERTA, CANADA

ASSESSING THE STATE OF INITIAL POST-FIRE VEGETATION REGENERATION FOLLOWING A SEVERE MONTANE WILDLAND FIRE

JESSE ASPINALL

Date of Defence: April 25, 2022

Dr. L. Chasmer	Associate Professor	Ph.D.
Dr. C. Hopkinson	Professor	Ph.D.
Co-Supervisor		
Dr. L. Flanagan	Professor	Ph.D.
Examination Committee Member		
Dr. C. Coburn	Professor	Ph.D.
Examination Committee Member		
Dr. D. Peddle	Professor	Ph.D.
Chair, Thesis Examination Committee		

ABSTRACT

This thesis utilized field and remote sensing methods to examine post-fire vegetation changes in moisture endmember sites within Waterton Lakes National Park, Alberta, Canada, following the 2017 Kenow Wildland Fire. Field data collected annually from 2018 to 2021 were used to validate multi-temporal RPAS and LiDAR datasets. Results indicate that biomass peaked in 2019, declining annually until 2021, corresponding with rising temperatures and below-average precipitation. RPAS optical imagery and Structure from Motion (SfM) effectively modelled vegetation height and biomass at the plot scale, while LiDAR active Normalized Burn Ratio (aNBR) effectively modelled biomass at the valley scale. Forest-based regression models indicated that proxies for moisture availability, like topographic position, distance to Cameron Creek, and elevation, influenced vegetation growth. This study demonstrated the utility of RPAS and LiDAR for quantifying post-fire vegetation regeneration across different scales and highlights the impact of moisture on vegetation recovery in this montane valley.

ACKNOWLEDGEMENTS

I would like to thank all those who supported me, both academically and personally, on this journey. My time at the University of Lethbridge has helped me grow, both personally and academically, and I owe a lot to the people around me.

First, thank you to my supervisors, Dr. Chasmer and Dr. Hopkinson. Your countless hours of editing, brainstorming, and guiding have made this work possible. Thank you for your support and patience over the years. Most importantly, thank you for the opportunity to collaborate with you as a student and research assistant. I have gained countless skills from the field to the lab, presented at national conferences, and learned so much, thanks to you. Second, thank you to my committee members, Dr. Coburn and Dr. Flanagan for your feedback and patience throughout this process. I value our discussion and the opportunity to collaborate with you over the years. Your contributions have helped better both me and this thesis.

A big thank you to everyone within the ARTeMIS and Peaters labs. This project includes data collected over four years with the help of so many great people. I would like to say a big thank you to Sam Gerrand and Travis Grant for showing up consistently over the summer of 2020, despite the long days, heat, and endless road construction. Thank you to Eric Rodvang who installed the permanent vegetation plots in 2018. Thank you to Adam Collingwood and Parks Canada for your support in the field and access to the study sites. A big thank you to everyone who helped both in the field, lab, and over Zoom: Thomas Porter, Celeste Barnes, Emily Jones, Chinyere Ottah, Danika King, Maxim Okhrimenko, Kailyn Nelson, Farnoosh Aslami, Humaira Enayetullah, Linda Flade, and Edberto Moura Lima.

I would like to acknowledge and thank the people who helped fund this research, including, Parks Canada funding for my support, provided to Drs. Hopkinson, Chasmer, and Flanagan,

NSERC Discovery Grant Program provided to Dr. Chasmer, NSERC SPG-N Canada Wildfire, Western Economic Diversification Canada to Chris Hopkinson, and the Canadian Foundation for Innovation to Chris Hopkinson.

Lastly, I would like to thank my family and friends for their steady support throughout both my undergraduate and master’s studies. Thank you to my wife, Shilo. You have listened to me ramble about LiDAR, practice numerous presentations, and have always been there to support me. I am fortunate to finish this process with you and begin the next chapter.

TABLE OF CONTENTS

LIST OF TABLES

LIST OF FIGURES

LIST OF EQUATIONS

CHAPTER 1: INTRODUCTION

2.1 BACKGROUND

Over the last half-century, fire seasons in Canada and regions across the northern Rocky Mountains, are beginning earlier in the spring and burning later into the fall, increasing the risk of extreme wildland fire behaviour (Hanes et al., 2019; Kirchmeier-Young et al., 2017; Westerling, 2016). Further, climate warming and moisture deficits combined with increasing fuel loads resulting from decades of suppression-based forest management have increased the proportion of severe wildland fires (Steel et al., 2018). Burn severity and climate, particularly moisture deficits, have significant influences on post-fire vegetation regeneration and can lead to post-fire succession trajectories that deviate from historic norms (Meng et al., 2015; Tautenhahn et al., 2016; Tepley et al., 2017). In the future, it is expected that post-fire ecosystems may transition from forest to grasslands, change dominant species, and experience a reduced capacity for long-term carbon storage (Bartowitz et al., 2019; Tepley et al., 2017). To model future post-fire vegetation regeneration under changing fire and climate conditions, there must also be an understanding of environmental and topographic influences that drive vegetation regeneration.

The collection of multitemporal remote sensing data provides information for large areas that are often difficult to access. These datasets can also be used to model the spatial distribution of vegetation characteristics, regeneration, and potentially, the environmental influences on growth. The overall objective of this study is to quantify the rates of post-fire vegetation change in moist and dry endmember sites over a 4-year period using field measurements, Remotely Piloted Aircraft Systems (RPAS), and airborne Light Detection and Ranging (LiDAR). This study will determine if RPAS and LiDAR methods can be used to detect changes in vegetation structure within the study sites and Cameron Valley bottom. If remote sensing methods effectively detect changes in vegetation, then vegetation growth will be modelled within the montane valley bottom.

A random forest predictive model will be used to identify environmental drivers of annual changes in vegetation.

2.2 POST-FIRE ECOSYSTEM SUCCESSION

Post-fire ecosystem recovery follows the theory of ecological succession, which is a predictable and well-understood process in which the vegetation structure changes over time (Odum, 1969). Initial post-fire ecosystems have a low Net Ecosystem Productivity (NEP) due to the high quantity of necromass left to decay on the forest floor, and the combustion of aboveground biomass available for carbon storage (Odum, 1969). In the first two to five years post-fire, rapid herbaceous vegetation growth increases the quantity of carbon stored in biomass through photosynthesis (Amiro et al., 2006; Odum, 1969). In montane environments like the Canadian Rocky Mountains, herbaceous vegetation provides shelter for establishing shade-tolerant seedlings, which become the dominant species as the ecosystem matures (Besnard et al., 2018; Larson & Franklin, 2005; Pedro et al., 2015; Reid et al., 2004). As ecosystems change, biomass accumulation and respiration balance and NEP becomes neutral (Odum, 1969). However, in mature forests, NEP may decrease as biomass peaks and competition for light and nutrients inhibits new vegetation growth (Potter et al., 2011).

Within montane forests of North America, wildland fires play a critical role in maintaining healthy ecosystems by removing organic matter from the forest floor, exposing mineral soils, increasing light availability, and returning nutrients to the soil, creating conditions suitable for the growth of new vegetation (Landhäusser et al., 2010; Tautenhahn et al., 2016; Tepley & Veblen, 2015; Zehetgruber et al., 2017). The time required for post-fire succession to reach the state of pre-fire carbon storage is dependent on the ecosystem and climate of the region (Potter et al., 2011). For example, in Yellowstone National Park, the time required for post-fire ecosystems to reach the state of pre-fire carbon storage ranged from 50 to 200 years (Potter et al., 2011). The capacity for the ecosystem to store carbon fluctuated annually due to increased biomass accumulation in moist years and reduced biomass accumulation in dry years (Potter et al., 2011).

Understanding rates of forest succession in the initial years following wildland fires, particularly in montane ecosystems which have highly variable climatic gradients, may improve the understanding of how ecosystems will recover from future wildland fires. Changing climate conditions and wildland fire regimes may prevent forests from reaching maturity or result in composition shifts such as from forests to grasslands, both of which would reduce the capacity of forests to store carbon (Bartowitz et al., 2019; Kashian et al., 2006; Tepley et al., 2017). The result of forests deviating from known successional trajectories could reduce ecosystem carbon storage, potentially altering both local and, if this occurs over larger areas, global climates.

2.3 CLIMATE AND WILDLAND FIRE REGIMES

Over the next century, the climate in Alberta, Canada is expected to warm by 1.2° C to 6.8° C, while annual precipitation is expected to increase from 21 mm to 60 mm (Jiang et al., 2017). Despite expected increases in precipitation, the temporal and spatial variation in precipitation is also expected to increase, potentially leading to longer and more frequent droughts (Jiang et al., 2017). Historically, rates of conifer establishment were highest in years with above-average snowpack and cool, wet summers compared to the mean (Andrus et al., 2018; Busby et al., 2020; Potter et al., 2011; Rodman et al., 2020; Rother & Veblen, 2017). Recent changes in precipitation, timing of snowpack melt, and air temperature could alter the distribution and species composition of montane forests. For example, a controlled study by Rother (2015) in the Colorado front ranges found that ponderosa pine (*Pinus ponderosa*) and Douglas-fir (*Pseudotsuga menziesii*) establishment and survival were greatest in plots with above-average precipitation. In contrast, establishment and survival were reduced in plots with above-average temperatures and average precipitation rates (Rother, 2015). Plots with increased air temperature and precipitation also showed declines in establishment and survival, though to a lesser degree than increased temperature alone (Rother, 2015).

A warmer, drier climate is also altering wildland fire regimes, which are defined as the pattern, frequency, and intensity of fires in a specific region over a prolonged period (Keeley, 2009). In western North America, wildland fire seasons have increased in length by approximately two weeks over the last 50 to 60 years (Hanes et al., 2019; Jolly et al., 2015; Kirchmeier-Young et al., 2017; Westerling, 2016). Wildland fire frequency and severity have also increased in Canada over the last half-century by three wildfires per year since 1959, leading to an approximately 34,000 ha yr^{-1} increase in the annual area burned (Hanes et al., 2019). Burn severity is classified by the loss of organic matter above or below ground and losses may occur during combustion or through decomposition in the years following the fire (Keeley, 2009). In some cases, burn severity has been classified based on specific levels of biomass loss where low severity burns are 0 – 20 %, moderate burns are 20.1 – 80 %, and burns are greater than 80.1 % (Larson & Franklin, 2005).

Wildland fires create ecosystem conditions that promote new vegetation growth by removing organic matter from the forest floor, exposing mineral soils, increasing light availability, and returning nutrients to the soil (Landhäusser et al., 2010; Tautenhahn et al., 2016; Tepley & Veblen, 2015; Zehetgruber et al., 2017). However, the influence of burn severity on post-fire vegetation regeneration varies based on regional conditions such as climate, topography, and species composition (Gordon et al., 2017; Larson & Franklin, 2005; Meng et al., 2015).

In montane ecosystems of North America, vegetation regeneration is greatest in regions of moderate to severe burns and lowest in the most severe and least severe burned regions (Gordon et al., 2017; Meng et al., 2018; Urza et al., 2017). Changes in fire regimes can influence post-fire vegetation regeneration for decades after a wildland fire occurs (Tautenhahn et al., 2016; Tepley et al., 2017). For example, large, severely burned regions contain fewer live tree islands and require seeds to be transported over a greater distance from the live tree edge, resulting in delayed establishment (Tautenhahn et al., 2016). Burn severity can also influence post-fire vegetation growth by altering micro-climate conditions such as canopy cover, soil composition, and the distribution of debris which impact moisture availability (Donato et al., 2009). Additionally, remaining standing dead canopies can increase shading and reduce evaporative stress at the ground surface (Minore, 1971). Bonnet et al., (2005) suggest that trees with more than 50 % of the crown burned will provide both shade and a source of scorched litter, resulting in a positive influence on the establishment of ponderosa pine. At the forest floor, burnt litter and debris can absorb or slow runoff, increasing moisture available for establishing conifer seedlings (Bonnet et al., 2005). In regions of low burn severity, mineral soils are not exposed which prevents seedlings from establishing, and the remaining canopy cover reduces light availability at the surface (Bonnet et al., 2005). In the most severely burnt regions, the remaining canopy cover and debris are reduced, increasing the evaporative stress on the forest floor (Bonnet et al., 2005).

It is understood that as drought conditions increase, the rates of post-fire establishment decrease, although this is dependent on species composition (Harvey et al., 2016; Rother et al., 2017). Drought conditions may result in successional lags, slowing the establishment of shade-tolerant species until a canopy provides shade, and moisture availability is increased (Gendreau-Berthiaume et al., 2018). Despite the current understanding of climatic influences on post-fire regeneration, the combined influence of changing climate and wildland fire regimes on post-fire succession is less understood. It is hypothesized that montane forest species composition and tree line elevation may change or that forests may transition to grasslands (Dodson & Root, 2013; Tepley et al., 2017). To understand how shifts in post-fire regeneration impact forests, habitats, and ecosystem services, there is a need to quantify the rate of vegetation re-establishment and the spatial variability based on environmental drivers. Continued monitoring of post-fire ecosystems is required to understand the degree to which change will occur, and how change will vary across different ecosystems.

2.4 TOPOGRAPHIC DRIVERS OF VEGETATION REGENERATION

The unique topography of montane ecosystems can create large variations in the distribution of post-fire vegetation regeneration. These variations are often associated with topographic micro-climates where temperature and moisture regimes can alter the regeneration trajectories of montane forests over space and time (Ireland & Petropoulos, 2015). Post-fire regeneration can be influenced broadly by elevation, and locally, by variations in micro-topography and aspect (Dodson & Root, 2013; McCaffrey & Hopkinson, 2020; Rother & Veblen, 2016).

Although the relationship between climate and elevation is dependent on the location of the ecosystem in question, it is expected that as climate warms, vegetation densities will increase at higher elevations if moisture is a non-limiting factor and soils are deep enough for establishment and survival (Dodson & Root, 2013; Rother & Veblen, 2016). For example, in the eastern Oregon Cascades, Dodson and Root (2013) determined that the probability of sampling a seedling below 600 m was less than 5 %, but 90 % above 1400 m. Similar observations were made in Yellowstone National Park, where four times more Douglas-fir and 12 times more lodgepole pine (*Pinus contorta)* seedlings were counted at higher elevations (Hansen & Turner, 2019). However, the impacts of elevation on vegetation regeneration are also dependent on latitude and the range of elevation considered in the study. Although climate conditions at higher elevations may be more suitable for establishment, higher elevations may represent a decrease in growing degree days, limiting the establishment and growth of vegetation.

In montane ecosystems, aspect-driven micro-climates can influence the accumulation of vegetation and often result in northern aspects having the highest rates of post-fire vegetation growth (Ireland & Petropoulos, 2015; Larson & Franklin, 2005; McCaffrey & Hopkinson, 2020; Meng et al., 2015). However, the influence of aspect varies based on species. For example, in the central Cascades Busby et al. (2020) determined that northeastern aspects had the highest overall tree density consisting of lodgepole pine, subalpine fir (*Abies lasiocarpa*) and Engelmann spruce (*Picea engelmannii*), while ponderosa pine, Douglas-fir and grand fir (*Abies grandis*) were found predominately on southwestern aspects. Increased shading on north-facing slopes reduces air temperature and increases moisture availability, making these regions more resilient to drought or the broader effects of climate change (Harvey et al., 2016).

2.5 REMOTE SENSING

Remote sensing is the process of collecting information related to electromagnetic energy that is reflected or emitted by a target (Shellito, 2023). Remote sensing technologies use energy emitted from the sun or generate their own source of electromagnetic energy to determine land cover, identify vegetation species, monitor plant phenology, and assess the vegetation health. and are often carried onboard satellites, aircraft, or RPAS platforms, and handheld cameras (Shellito, 2023). The use of remotely sensed data, combined with field validation, provides an opportunity to observe changes in vegetation structure and plant physiology based on spatially continuous optical data over large, often inaccessible areas. Satellite optical imagery is measured across a variety of spatial resolutions, making it ideal for covering the full extent of burn areas and capturing the spatial variability of burn severity. Optical imagery is the primary method for monitoring vegetation and determining burn severity using spectral indices such as the Normalized Difference Vegetation Index (NDVI) or difference Normalized Burn Ratios (dNBR) (Meng et al., 2015). Although optical remote sensing is a valuable tool for monitoring vegetation, the process of compositing images or cloud masking can omit data and contribute to errors, particularly in regions of sparse vegetation, such as early post-fire ecosystems, which are prone to higher error compared to established forests (Storey et al., 2016; Zhao et al., 2016). While satellite optical remote sensing is a valuable tool for detecting long-term changes, this thesis focuses on the use of high spatial resolution RPAS imagery and airborne LiDAR. These technologies provide the opportunity to combine spectral properties with estimates of vegetation structure (Chasmer et al., 2014).

Active remote sensing methods such as LiDAR provide users with control over data collection schedules, allowing for collection in ideal conditions, and offering users a remote sensing approach that differs from satellite optical remote sensing. LiDAR sensors emit laser pulses from an airborne platform toward the Earth's surface where pulses interact with the ground targets and the sensor measures returned energy (Lim et al., 2003). The time difference between laser pulse emission and return provides the range between the sensor and the surface (Lim et al., 2003). A differential Global Positioning System (dGPS) and an Inertial Measurement Unit (IMU) measure the location and orientation of the aircraft, while a precision clock measures the time interval between a LiDAR pulse and return (Dong & Chen, 2018; Lim et al., 2003). Based on the location of the LiDAR system and the measured time interval between pulse emission and return, x, y, and z coordinates can be determined for every pulse that reflects from the surface (Dong & Chen, 2018). Each LiDAR pulse has a footprint, or area of pulse contact with the surface, typically ranging from 10 cm to 30 cm depending on flying height (Beland et al., 2019; Hopkinson et al., 2006). As a laser pulse contacts the surface, the energy interacting with varying objects within each footprint can be split into multiple returns, producing a point cloud (Beland et al., 2019). The result is a 3D surface where each point has a horizontal and vertical position and an intensity value indicating the amount of returned energy (Lim et al., 2003).

Historically, airborne LiDAR systems have used a singular channel, typically 1064 nm or 1550 nm. The recent introduction of multispectral LiDAR systems allows for the utilization of multiple laser intensities (532 nm, 1064 nm, 1550 nm) to capture different reflection characteristics from varying surfaces (Hopkinson et al., 2016). The combination of multiple laser intensities increases the ability to classify vegetation based on the return intensity or compute vegetation indices (Chasmer et al., 2017; Hopkinson et al., 2016; Okhrimenko et al., 2019; Orkhrimenko & Hopkinson, 2019).

The combination of LiDAR structural and spectral properties is an effective method for modelling vegetation structure including height and cover (Hopkinson et al., 2006). However, LiDAR has not been frequently used in initial post-fire ecosystems where the variance in vegetation height is significantly less than that of a mature forest. If LiDAR methods can be used to estimate vegetation growth in initial post-fire ecosystems, it could be an effective tool for quantifying spatially and temporally varying vegetation growth rates at the landscape scale, and identifying some of the environmental factors that influence post-fire vegetation growth.

Although LiDAR data can be used independently, it may also be used to scale detailed local information to larger regions when combined with optical remote sensing such as Landsat (Garcia et al., 2017; Meng et al., 2018). Similarly, RPAS may be an effective tool for scaling plot-level data to larger-scale LiDAR datasets. RPAS platforms facilitate high spatial (and sometimes spectral) resolution image collection over small areas and can provide a cost-effective alternative to other remote sensing and field methods (Alexiou et al., 2021). Recent developments in RPAS data management have combined the benefits of high-resolution optical imagery and the production of 3D point clouds based on overlapping RPAS image photogrammetry, which often includes visible wavelengths and other additional wavelengths, such as NIR that can be used for the derivation of greenness and vegetation indices. Photogrammetry uses two or more overlapping images of a feature taken from different positions to create a 3D image that can be used to measure height (Linder, 2006). On the other hand, photogrammetrically derived point clouds based on Structure from Motion (SfM) have been shown to accurately quantify forest canopy height and tree diameter within open canopies (Chen et al., 2017; Goodbody et al., 2018; Larrinaga & Brotons, 2019). SfM uses a computer-automated process to tie together key points from overlapping 2D images, creating a 3D point cloud comparable to LiDAR data (Dandois & Ellis, 2010). Given the uncertainty of the ability of LiDAR to model initial post-fire herbaceous vegetation, RPAS may provide an effective intermediate remote sensing technology that could be used to scale plot-level data to a montane valley.

2.6 STUDY OUTLINE

Climatic changes in montane regions of western Canada are impacting wildland fire regimes and post-fire vegetation regeneration. The scale of these impacts on early post-fire regeneration is not well understood in regions where fire suppression has been used to manage the landscape. Additionally, topographic gradients in montane environments can result in significant variations in moisture availability. The influence of moisture availability on post-fire vegetation regeneration under changing climatic conditions is also not well understood. To address these unknowns, this thesis aimed to quantify rates of post-fire vegetation regeneration in two moisture endmember sites over the first four years following a severe montane wildland fire in a region that has undergone a century of fire suppression. To do this, bi-weekly measurements of vegetation height and cover, and annual biomass harvests were conducted across two sites, providing insight into spatial and temporal changes in rates of vegetation growth. To determine broad variability in vegetation growth rates, RPAS optical imagery and SfM photogrammetry were compared with coincident field measurements. To understand the influence of moisture on vegetation regeneration at the montane valley scale, multitemporal LiDAR was used to model vegetation height and biomass within the Cameron Valley bottom, Waterton Lakes National Park, Alberta, Canada. The primary objectives of this thesis include:

1. Examine and compare rates of post-fire vegetation growth in two moisture endmember sites over the first four years following a severe montane wildland fire.
    a. Following a severe wildfire, do moist montane valley sites enhance the rate of herbaceous vegetation recovery compared to drier sites?
    b. If they do, will there also be greater conifer tree establishment in moist sites?
    c. Determine if RPAS optical imagery and SfM photogrammetry can capture variability in post-fire vegetation regeneration (specifically height and biomass) in the first four years following a severe wildland fire.
2. Develop LiDAR methods to model biomass at the valley-scale and model topographic influences (as an indicator of moisture) on the spatial distribution of vegetation.
    a. Assess the efficacy of airborne LiDAR canopy height models for capturing variability in post-fire vegetation structures (specifically height) in the first four years following a severe wildland fire.

b. Use harvested plot biomass to develop a model of post-fire biomass change over the first four years of post-fire vegetation regeneration in the Cameron Valley.
c. Use the thematic information derived from airborne LiDAR within a machine learning framework to identify abiotic environmental factors that may influence biomass accumulation in the Cameron Valley following a severe wildland fire.

2.6.1 Study area

This study focused on vegetation regeneration following the Kenow Wildland Fire (2017) in Waterton Lakes National Park, Alberta, Canada (hereafter 'Waterton') (114° 2' 24" W, 49° 1' 58" N) (Figure 1.1). Waterton is part of the southern Canadian Rocky Mountains (CRM), which are an important part of Canada's history, economy, and natural landscape. The CRM is home to five National Parks that hosted approximately eight million visitors in 2019/20, accounting for 33 % of all Parks Canada visitors (Government of Canada, 2020). Waterton consists of four ecoregions that span from the Foothills Parkland (1280 m - 1500 m), composed of rough fescue (*Festuca scabrella*) and aspen (*Populus tremuloides*), to the barren Alpine Ecoregion (2250 m - 2700 m) (Parks Canada, 2018a). Waterton is a diverse region with approximately 1000 species of vascular plants, including 175 provincially rare species, 50 nationally rare species, and 20 species only found in Waterton (Parks Canada, 2018a).

The rich ecosystem diversity in Waterton is due to the topographic gradients and regional atmospheric conditions associated with its location in the southeast corner of the Canadian Rocky Mountains. The mixing of warm, moist air from the Pacific coast with cold, dry Arctic air results in Waterton receiving the highest annual precipitation in Alberta. Precipitation ranges from 1072 mm annually in the Parkland Foothills to 1524 mm towards the Rocky Mountain Continental Divide and consists of approximately 50 % snow and 50 % rain (Parks Canada, 2018b). Elevation gradients also drive strong winds throughout Waterton, with wind speeds averaging 30 km/hr daily and gusts reaching over 150 km/hr mild (Parks Canada, 2018b). Air temperature ranges from a minimum of - 38° C in the winter to a maximum of 35° C in the summer. To summarize the climatic conditions of Waterton, it is best characterized as wet, windy, and mild (Parks Canada, 2018b).

This study concentrated on two sites in the Cameron Valley, Waterton: A moist site (114° 2’ 18” W, 49° 2’ 4” N and 1632 m.a.s.l) and a dry site (114° 2’ 27” W, 49° 1’ 51” N and 1656 m.a.s.l) (Figure 1.1 C). These sites were selected to represent moisture endmembers within the Cameron Valley and used to assess variation in vegetation regeneration based on moisture availability. Prior to the Kenow Wildland Fire, this region was dominated by mature lodgepole pine, subalpine fir, and Engelmann spruce (Parks Canada, 2018a). Fire regimes in Waterton are influenced by more than 100 years of fire suppression, and Cameron Valley had no history of natural or prescribed burns in the last century (Parks Canada, 2021).

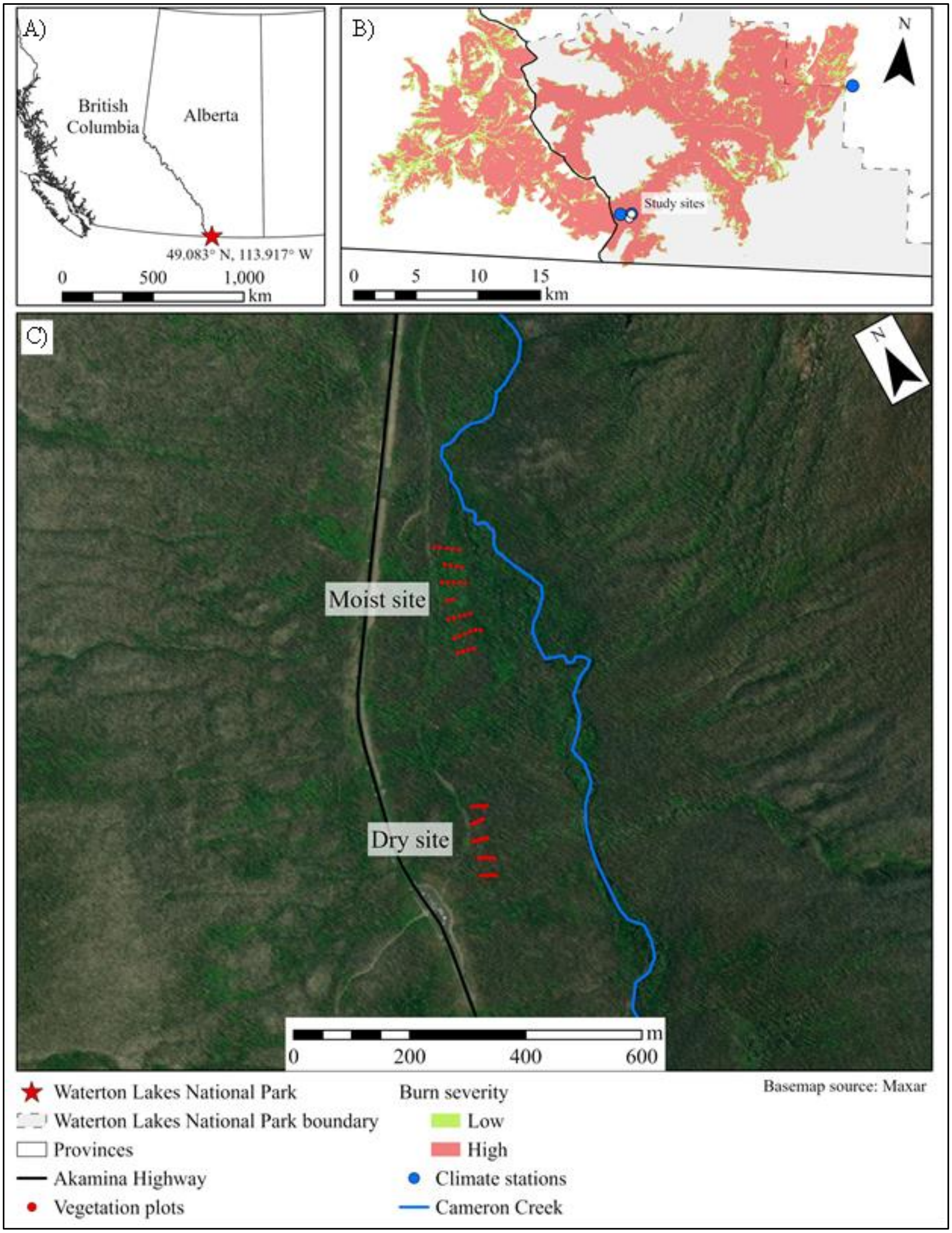

Figure 1.1 Location of Waterton Lakes National Park within Canada (A), including the burn extent and severity of the Kenow Wildland Fire (2017) in Waterton Lakes National Park (B), and the location of the moist and dry study sites within the Cameron Valley (C).

2.7 THESIS STRUCTURE

This thesis consists of four chapters (including the current introduction). Chapter two addresses the first objective of the thesis and compared rates of post-fire vegetation growth in two moisture endmember sites over the first four years following a severe montane wildland fire. This chapter quantifies the changes in measured vegetation structure (height, cover, and species) over four years, the spatial variability in soil conditions (moisture and bulk density), and interannual changes in air temperature and precipitation, including two abnormally hot, dry summer periods. Field measurements were then compared with RPAS SfM modelled vegetation height and gcc. Chapter three addresses the second objective of this thesis and focused on developing biomass models to quantify rates of post-fire vegetation regeneration and identify environmental drivers of regeneration using airborne LiDAR data. Chapters 2 and 3 are written in ‘journal article’ format (excluding abstracts) with the expectation that these may be published. Chapter four concludes the thesis by providing a summary of chapters two and three, a discussion of the applications and limitations of this study, and recommended considerations for future research related to this topic.

CHAPTER 2: STATE OF REGENERATION: EARLY POST-FIRE SUCCESSION FOLLOWING A SEVERE MONTANE WILDLAND FIRE IN WATERTON LAKES NATIONAL PARK

3.1 INTRODUCTION

Anthropogenic climate change is causing wildland fire behaviour to deviate from historical norms, resulting in increases in fire severity and intensity, fire frequency, and area burned (Hanes et al., 2019; Jolly et al., 2015; Kirchmeier-Young et al., 2017). The associated combustion of large quantities of biomass can have detrimental impacts on communities both locally and with distance from fires, due to the various chemical and soot emissions (Amiro et al., 2001). Beyond the initial impacts of wildland fire, post-fire ecosystems are recovering under climatic conditions dissimilar to conditions at the time of pre-fire ecosystems development. The combination of changing wildland fire behaviour and increasing atmospheric aridity is expected to alter the distribution of vegetation and species composition, particularly in montane ecosystems which have high variability in microclimate conditions.

Although wildland fires are an essential component of maintaining a healthy montane ecosystem, increasing burn severity and burn patch size reduce the area suitable for regenerating vegetation (Donato et al., 2009; Tepley et al., 2014). The regeneration of vegetation after a fire is significantly affected by changing climate conditions (Andrus et al., 2018). Above-average accumulation of snowpack and cool, wet summers are strongly linked to the establishment and survival of post-fire vegetation (Andrus et al., 2018). Although precipitation is expected to increase over the next century, it is anticipated that increases will be spatially and temporally variable, raising the likelihood of drought (Jiang et al., 2017). Previous assessment of conifer establishment in montane environments indicates that even with higher rates of precipitation, increasing temperatures will lead to decreases in seedling establishment and survival (Rother, 2015). Transitions to warmer seasons and greater evaporative losses in the Canadian Rockies (and other montane areas in western North America) have shifted forest expansion to higher elevations and north-facing slopes where moisture availability is greater (Dodson & Root, 2013; Landhausser et al., 2010; McCaffrey & Hopkinson, 2020; Tepley et al., 2017).

Initial post-fire vegetation regeneration in montane forests of North America consists of rapid vegetation growth that transitions to conifer or deciduous forests as the ecosystem recovers (Odum, 1969). Rapid herbaceous vegetation growth is positively influenced by increased light availability at the forest floor and aids in balancing post-fire carbon losses (Fellow et al., 2018; Goulden et al., 2011). Herbaceous vegetation provides shelter for establishing shade-tolerant conifer seedlings, which grow above herbaceous vegetation after several years, and increase the quantity of long-term carbon storage within the ecosystem (Besnard et al., 2018; Larson & Franklin, 2005; Pedro et al., 2015; Reid et al., 2004). Despite the hydro-climatic changes that have occurred over the last few decades, few studies have examined the implications of moisture availability on initial post-fire regeneration in Canadian montane ecosystems. This is important as moisture provides an indicator of how climatic drying could impact montane ecosystem regeneration following future fires.

Montane post-fire ecosystems are often difficult and hazardous to access, making remote sensing technologies such as Remotely Piloted Aircraft Systems (RPAS) important tools in understanding vegetation regeneration. Remote sensing systems enable the acquisition of data over areas that are larger than standard forest mensuration plots (400 m^2) and systems such as RPAS offer a cost-efficient approach to collecting high spatial-resolution optical imagery. Recent developments in RPAS photogrammetry using Structure from Motion (SfM) allow for the creation of three-dimensional (3D) point clouds that provide vertical and horizontal measurement of vegetation (Dandois & Ellis, 2010). RPAS SfM data has been used to monitor coarse woody debris and post-disturbance vegetation regeneration, but there is little research on the application of RPAS imagery and SfM within initial post-fire ecosystems (Bohlin et al., 2017).

This study examines vegetation growth during the first four years following the Kenow Wildland Fire (2017) in Waterton Lakes National Park, Alberta, Canada, a region which has undergone 100 years of fire suppression (Parks Canada, 2021). Vegetation plots were established in a moist and dry area of Cameron Valley to represent moisture endmembers and capture variation in vegetation structure and species richness. The goal of this study was to examine and compare rates of post-fire vegetation growth in two moisture endmember sites over the first four years following a severe montane wildland fire by addressing the following questions: (i) following a severe wildfire, do moist montane valley sites enhance the rate of herbaceous vegetation recovery compared to drier sites? (ii) If they do, will there also be greater conifer tree establishment in moist sites? (iii) Determine the ability of RPAS optical imagery and SfM photogrammetry to quantify the variability in post-fire vegetation height and biomass in the first four years following a severe wildland fire.

3.2 MATERIALS AND METHODS

3.2.1 Study area

This study was conducted within the most southerly part of the Canadian Rocky Mountains in the Cameron Valley of Waterton Lakes National Park (hereafter ‘Waterton’) (114° 2’ 24” W, 49° 1’ 58” N), Alberta, Canada (Figure 2.1A). The Kenow Wildland Fire started on August 30, 2017, from a lightning strike during an intense thunderstorm west of the Waterton boundary (Parks Canada, 2019). On September 11, 2017, abnormally warm air temperatures and high winds drove the Kenow Wildland Fire through Waterton, consuming a total of 35,000 ha, including 19,300 ha (38 %) of Waterton (Parks Canada, 2019). The high severity of the Kenow Wildland Fire combined with fire suppression over the last century, provided a unique opportunity to quantify the impacts of fire severity on post-fire regeneration within this montane environment.

Waterton has a diverse region that hosts over 1000 species of vascular plants covering a range of ecoregions from foothills parkland to alpine (Parks Canada, 2018a). Temperature and precipitation gradients are driven by a variety of factors, including atmospheric systems (over broad areas) and more locally, large topographic variations from the Rocky Mountain Continental Divide to the prairie parkland. Before the Kenow Wildland Fire, forests of the Cameron Valley were mature (older than 100 years) with no recorded natural or prescribed burns (Parks Canada, 2021). The montane and subalpine ecoregions of Waterton are dominated by lodgepole pine (*Pinus contorta*), subalpine fir (*Abies lasiocarpa*), and Engelmann spruce (*Picea engelmannii*) (Parks Canada, 2018a). The depth of burn ranged from an average of 13.3 cm (maximum = ~42 cm) in the dry site to 18.2 cm (maximum = ~52 cm) in the moist site (Gerrand et al., 2021).

Two sites were selected to represent nearby forested topographical and moisture variations found in the Cameron Valley bottom (Figure 2.1C & D). Meteorological instrumentation, an eddy covariance system, and vegetation plots were established in a moist riparian part of the Cameron Valley (hereafter ‘moist site’: 114° 2’ 18” W, 49° 2’ 4” N and 1632 m.a.s.l) (Figure 2.1 C; Figure 2.2). This site is located approximately 60 m west of the perennial body of Cameron Creek and remains moist for most of the year due to intermittent streams that branch off Cameron Creek and run through the eastern side of the site. Other smaller intermittent creeks flow through rills from the mountainsides and into the site, contributing additional moisture in the early part of the growing season (Figure 2.2A. This occurs until approximately the end of June and intermittent creeks dry up in the latter part of the summer. Additionally, an intermittent groundwater spring floods the southern part of the site until late June when the last of the snow at the higher elevations has melted.

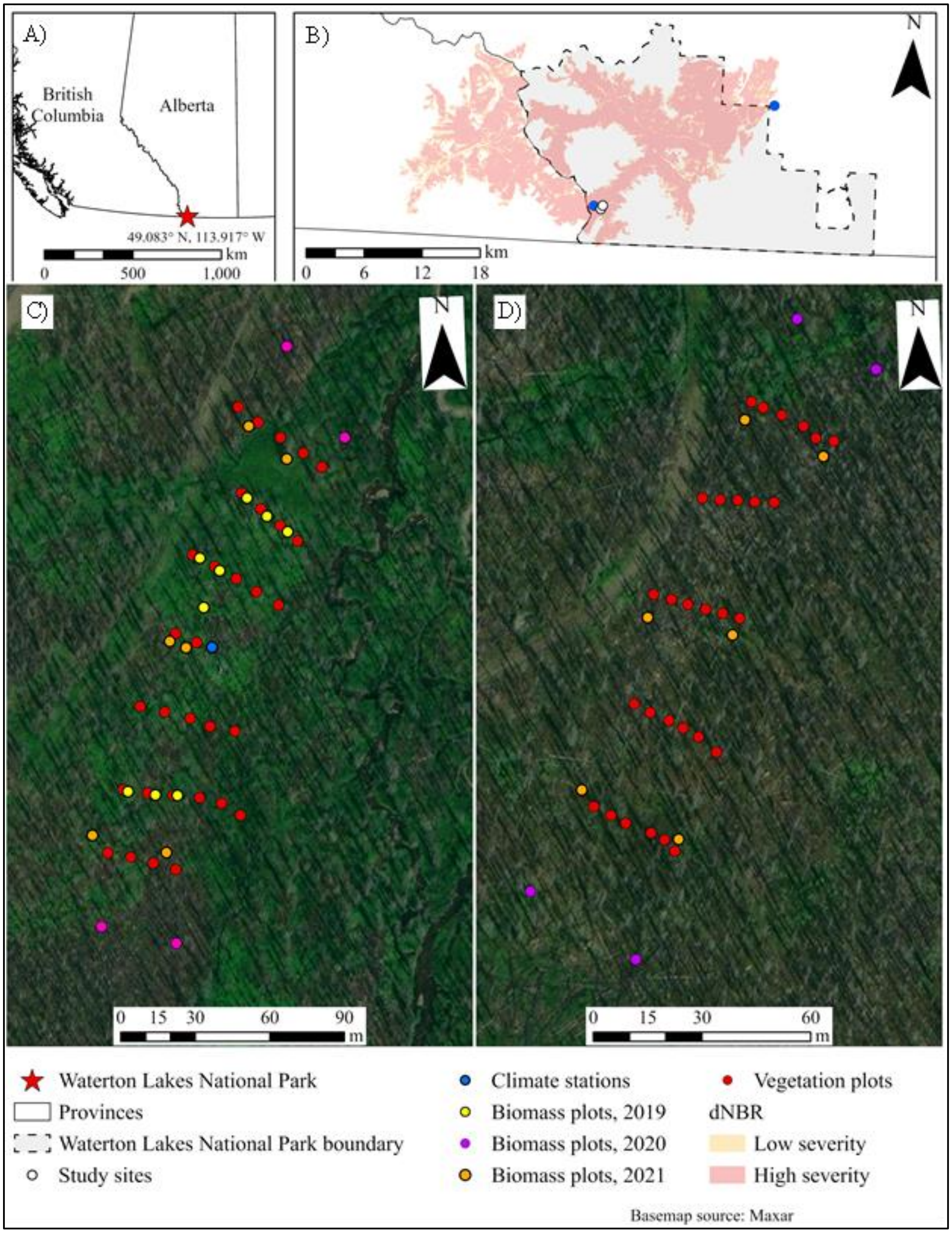

Figure 3.1 A) Location of Waterton within western Canada; B) location of two study sites and severity of the Kenow Wildland Fire shown as a Landsat OLI-derived differenced Normalised Burn Ratio (dNBR); C) The location of biomass and vegetation plots within the moist study site; D) The location of biomass and vegetation plots within the dry site, both of which are positioned over a basemap image from Earthstar Geographics (Maxar).

The slope of the moist site ranges from 1° to 9° (average = 4°, standard deviation (SD) ± 2°) and is east-facing. The soil composition in the moist site is organic and has a silty texture with some exposed mineral soils in the southernmost transect of vegetation plots. The average Volumetric Water Content (VWC), obtained from 124 vegetation plot measurements between July 12th and August 4th, 2020, was 14 % (SD ± 10 %). Dominant post-fire herbaceous species in this site include thimbleberry (*Rubus parviflorus*), Kentucky bluegrass (*Poa pratensis*), and white spirea (*Spiraea betulifolia*). Species richness varied from 34 species in 2018 to 24 species identified in 2020.

In July 2020, a second site (hereafter 'dry site') was established in a drier, slightly upraised area of the Cameron Valley, approximately 350 m south of the moist site (114° 2' 27" W, 49° 1' 51" N and 1656 m.a.s.l) (Figure 2.1 D; Figure 2.2B). The dry site is approximately 175 m west of Cameron Creek and free of rills and depressions that hold late spring snowpack or accumulate runoff. The slope in this site ranges from 1° to 13° (average = 5°, SD ± 3°) and is mostly east facing. Soil composition is predominately composed of rocky, mineral soils with shallow organic layers in the southern transects. The average VWC between July 12th and August 4th, 2020, was 8 % (SD ± 5 %) and is significantly F (1,221) = 29.8, $p < 0.001$) drier than the moist site. Herbaceous vegetation cover is sparse compared to the moist site, with only nine species identified, and is dominated by fireweed (*Chamaenerion angustifolium*), with few other species present.

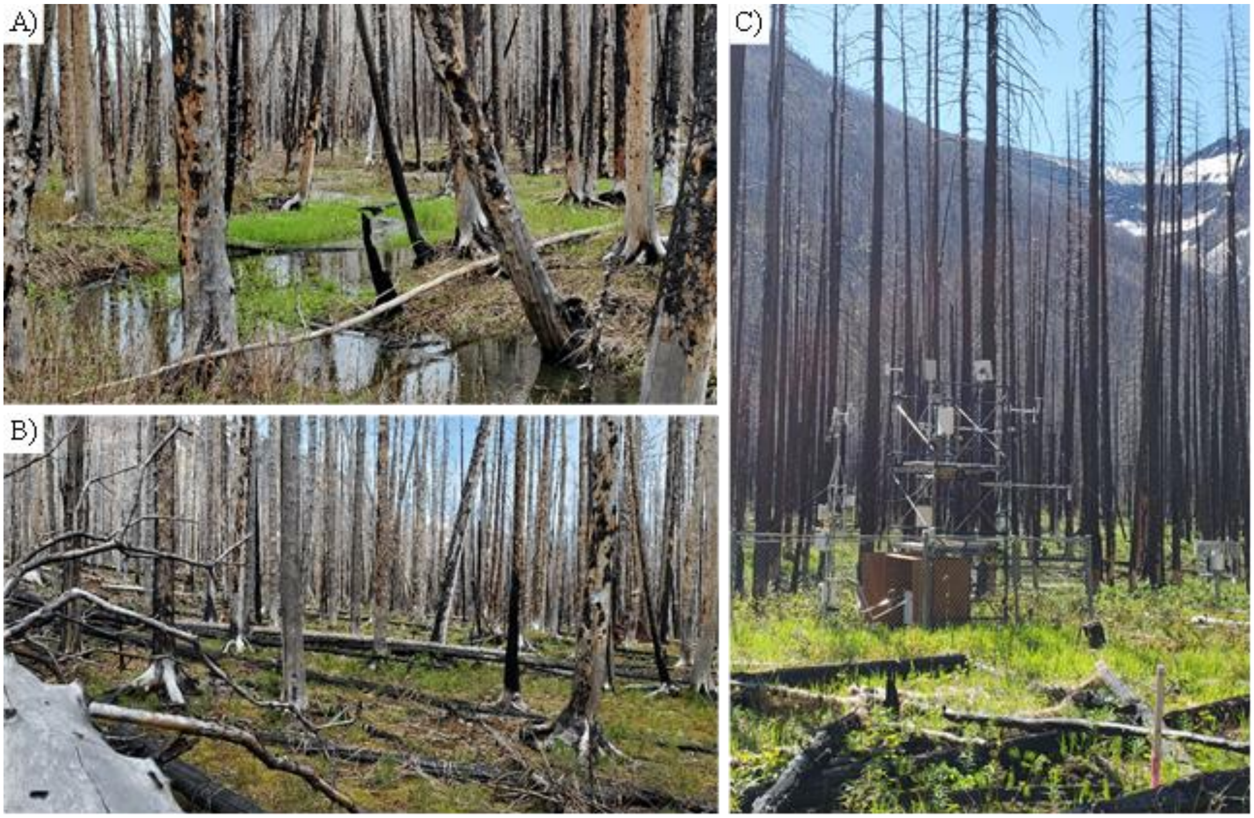

Figure 3.2 Image A) shows intermittent flooding in the moist site that is present until approximately late June, B) shows the dry site, and C) shows the HMP45C shielded temperature/relative humidity probes located in the moist site.

3.2.2 Meteorological data collection

Localized meteorological and soil moisture data were collected within the moist site (in addition to plot level VWC measurements at both moist and dry sites), including precipitation data (Geonor all-weather cumulating precipitation – rain gauge; Geonor, United States) from October 2018 to September 2021. Air temperature data for the moist site were acquired using Campbell Scientific Inc. HMP45C shielded temperature/relative humidity probes located at a height of approximately two meters from the ground surface (Figure 2.2 C). Climate data were used to compare the timing and quantity of precipitation at the study sites from 2019 to 2021. Here, it was assumed that precipitation and air temperature did not vary greatly between the two sites as they are only 350 m apart.

Climate data gathered at the Waterton Park Gate Climate Station (Environment Canada, 2022) was used to represent annual deviations from the long-term mean for both precipitation and temperature. Although there are climate differences between Cameron Valley and the Park Gate caused by topographic variation, the Park Gate provides the longest record in the region. It was assumed that climate anomalies experienced at the Park Gate would also occur within the Cameron Valley, located within 18 km of the long-term meteorological station. Annual variations in temperature were compared with the 45-year mean, while water year (October - September) total precipitation data were compared with the 25-year mean. Additionally, Snow Water Equivalent (SWE), temperature, and precipitation data were acquired from the Akamina 2 climate station located approximately 750 m to the west of the study sites (Agriculture and Irrigation, Alberta Climate Information Service (ACIS), 2021). SWE is the quantity of water present within the snowpack and is calculated based on changing levels of antifreeze in a standpipe connected to a snow pillow (Alberta Environment and Parks, 2018).

Within the moist site, 31 permanent vegetation plots (1.2 x 1.2 m, due to the use of a camera photo frame, which was positioned over each plot, making it easier to identify the plot boundary) were established in September 2018 (Figure 2.3). Plots were distributed in a northeast-to-southwest orientation over seven transects, with 10 m between plots and 30 m between transects. The orientation and distribution of the plots were determined by considering the location of an eddy covariance system deployed at the site. Plots were arranged within the flux footprint in the upwind and downwind directions to effectively capture the contribution of carbon dioxide and water fluxes between regenerating vegetation and the atmosphere. Vegetation plots were measured and photographed three times throughout September 2018, approximately bi-weekly from May

29th to September 11th, 2019, July 12th to August 18th, 2020 (with a shortened sampling window due to COVID-19 constraints), and from June 11th to September 26th, 2021.

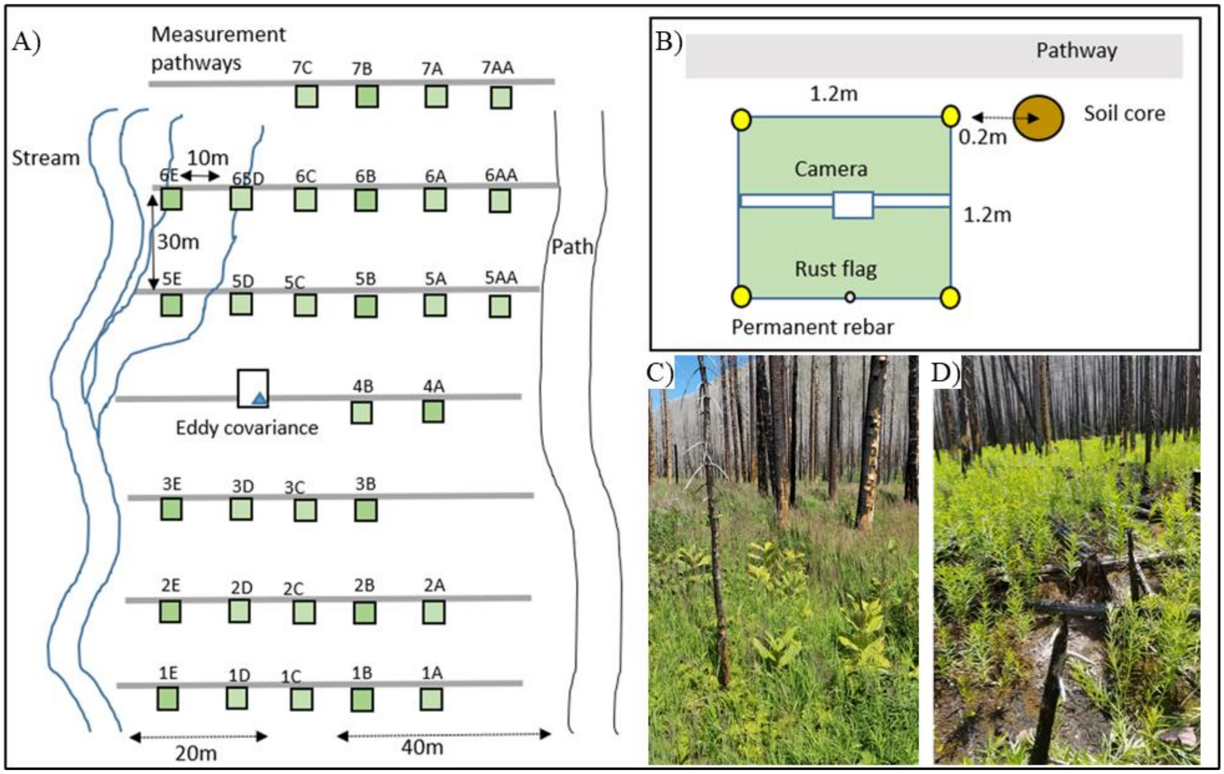

Figure 3.3 A) Plot distribution at the moist site, established in 2018. B) Setup of individual plots including pathway, consistently used as to not disturb surrounding vegetation, location of the cameras metal frame, and location of soil cores. C) Image of the moist site taken in 2020, looking north from the eddy covariance tower. D) Image of the dry site taken in 2020, looking east at the center of the site.

Due to the interest in comparing regenerating vegetation across moist and dry sites within the Cameron Valley, 29 additional vegetation plots were established in the dry site in July 2020. The dry site consisted of five transects with 5 m between plots and 30 m between transects, with the same directionality as the moist site. Plots within the dry site were measured approximately bi-weekly in July and August 2020 and from June to September 2021. All plots were located using a Topcon Inc. (Canada) HiPer SR II survey-grade Global Navigation Satellite System (GNSS), with a base station located within 500 m of both sites.

The maximum vegetation height was measured at the left, center, and right side of the center line of each plot, when facing north, using an extendable measuring stick. Vegetation cover was estimated by counting point intercepts with the measuring stick at each height measurement location. Each layer of vegetation that contacted the measuring stick was counted as an intercept following the point intercept method (Caratti, 2006). During the summers of 2018 and 2020, species within the vegetation plots were identified and their proportional cover within the plot was visually estimated. In 2020 and 2021, conifer seedlings in each plot were counted to determine the conifer density within each study site. Finally, VWC (%) was measured in the same locations as vegetation height using a Hydrosense 2 Handheld Soil Moisture Sensor (Campbell Scientific Inc.). VWC data were collected at irregular times (3 of 6 site visits in 2019, 4 of 5 site visits in 2020, and 0 of 5 site visits in 2021) throughout the study period due to probe availability.

In addition to these measurements, photographs were taken using a visible wavelength (red, green, blue; hereafter, RGB) digital camera to estimate cover and as a proxy indicator of vegetation productivity over time (based on the proportion of foliage vs. soil in each photograph). For consistent image collection, the camera was mounted on a metal frame that was placed around the corners of the plots, such that each corner was 1.2 m from the corners adjacent to it (Figure 2.3). Photographs were taken from above each plot, looking directly down, to cover the full area of the plot and were taken from a height of approximately 1.8 m ± 0.2 m. To maintain consistent light conditions during cloud-free or intermittent cloudy days, an umbrella was used to simulate consistent, diffuse cloud cover. Plots were photographed during each visit to the study sites and all photos were taken within four hours of each other. Images were used to calculate the Green Chromatic Coordinate (gcc) of each plot (Badgley et al., 2017; Nijland et al., 2014; Sonnentag et al., 2012). Gcc is the measure of greenness within an image and is used to track phenology and plant health (described below).

To determine the spatial variability of the post-fire soil characteristics between moist and dry sites, soil cores were collected in August 2020 and used to calculate the soil bulk density. Soil cores were collected using an AMS soil core sampler kit with hammer attachment (AMS, United States) and three liner inserts (each measuring 4.8 cm diameter and 5 cm depth). Soil cores were located approximately 15 - 20 cm outside of the southwest corner of each vegetation plot and were collected in three depth intervals (0 - 5 cm, 5 – 10 cm, and 10 - 15 cm). Each depth interval was separated by cutting the soil between the liner inserts and stored individually to identify changes in bulk density with depth. In the moist site 31, 30, and 28 cores were collected for each depth interval, and in the dry site, 23, 22, and 15 samples were collected for each depth interval (0 - 5 cm, 5 - 10 cm, and 10 - 15 cm respectively).

The variability of biomass accumulation within and between the two sites was measured by harvesting living biomass within plots. In September 2019, nine biomass plots were established in a systematic pattern to reflect the vegetation growth in the moist study site (Figure 2.1 C). In 2020, eight biomass plots were established between the moist and dry sites (Figure 2.1 C & D). Plots were located at the four corners of each site, 30 m north or south of the end transect to limit the potential impacts of harvest on fluxes estimated by eddy covariance in the moist site. In 2021, 12 biomass plots were systematically distributed to represent the north, center, and south end of the moist and dry sites (Figure 2.1 C & D). All biomass plots were 1 x 1 m in size and located using survey grade GNSS with an accuracy of < 0.10 m, such that biomass could be compared with RPAS optical imagery and SfM data. All vegetation within the plots were clipped at the ground surface and stored in large paper bags for lab analysis.

3.2.3 RPAS data collection

RPAS image data were collected bi-weekly throughout the fall of 2018, summer of 2019, and summer of 2021 using either the Mavic Pro v1 (2018) or Mavic Pro2 (2019 onwards) (Figure 2.4). No RPAS image data were collected during the summer of 2020 due to COVID-19 restrictions and construction within the Cameron Valley. Flights with survey parameters described in Table 2.1 were conducted with a forward tilt of 15° to enhance vertical sampling and at a height of 40-50 m above the ground surface. Speeds varied from 2.5-4.0 m s^{-1} with a 75-90 % front overlap and 70-90 % side overlap. Speed and overlaps were varied to accomplish a full flight on a single battery, with minor adjustments for lighting and wind conditions on any given day.

Table 3.1 Specifications of RPAS used and output pixel spatial resolution.

Year	RPAS and camera used	Orthomosaic ground sample distance (cm)	Average point density (Points m^{-2})
2018 moist site	Mavic Pro v1 - 4MP	1.16	688
2019 moist site	Mavic Pro2 - 20MP	0.89	1253
2021 moist site	Mavic Pro2 - 20MP	1.40	480
2021 dry site	Mavic Pro2 - 20MP	1.22	766

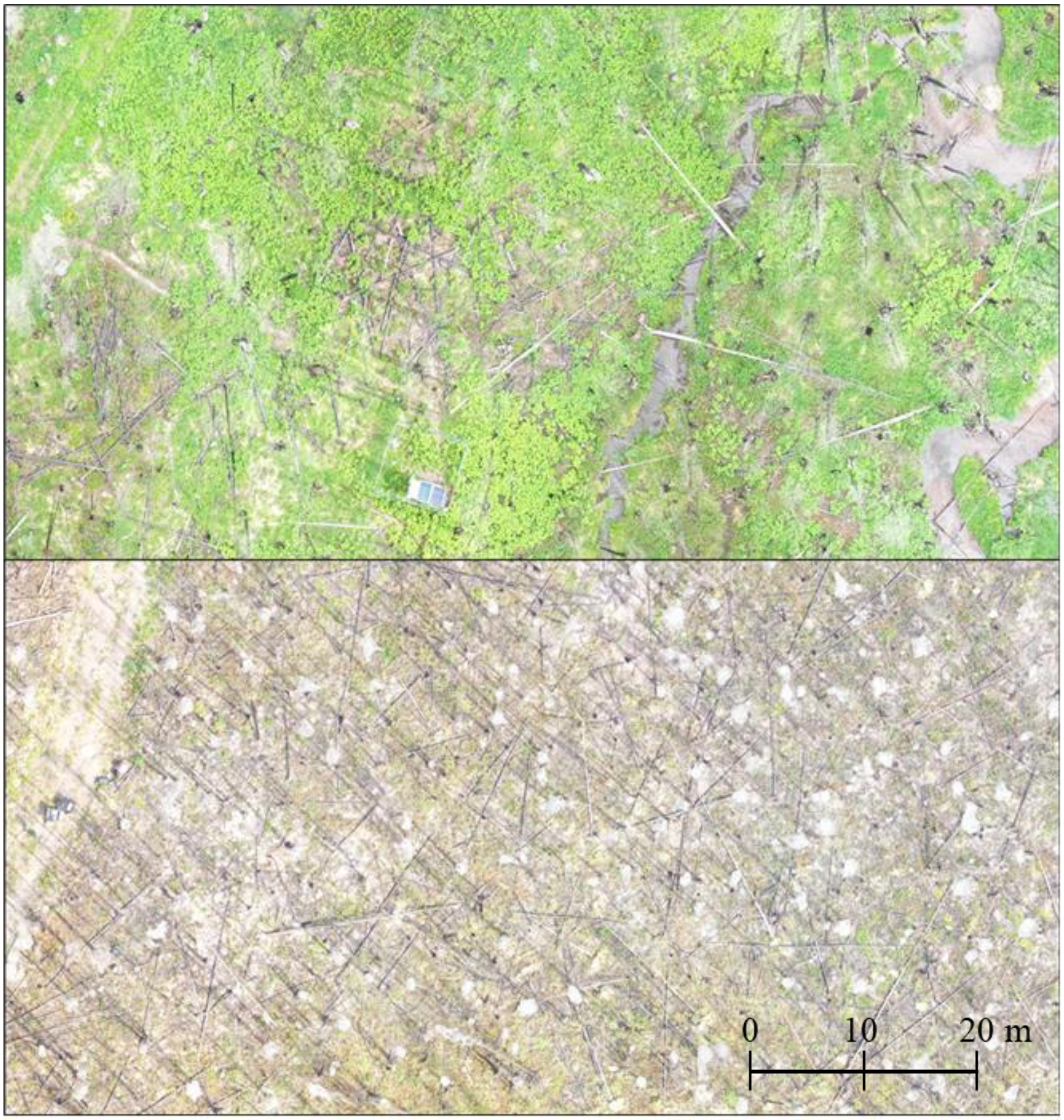

Figure 3.4 Mosaicked downwards looking photographs of the moist (top) and dry (bottom) study sites using a Mavic Pro V2 RPAS system collected on July 29, 2021.

3.3 DATA ANALYSIS

3.3.1 Vegetation plot and soil data analysis

Vegetation height and cover measured in the field were determined per plot and day by calculating the average and standard deviation of the three measurements at the left, center, and right side of the plot. Plot photographs, which were used to estimate the proportions of green vegetation vs. soil/scorched ground (Figure 2.5) were processed in ArcMap and ArcGIS Pro (ESRI, United States), to create shapefiles. These were used to consistently capture the same area and bounds of the photograph within each vegetation plot and to extract the digital numbers (DNs) in each of the three RGB image bands. Statistics, including the average and standard deviation, were determined for each image band within the extracted photo area. Areas where direct sunlight was captured in the image were masked and excluded from the statistical analysis. Raster calculator was used to determine the gcc values for each image:

$$gcc = \frac{G}{(R + G + B)} \qquad \textbf{[Equation 3.1]}$$

Where R represents the red band, G represents the green band, and B represents the blue band within each clipped photograph. Vegetation height and gcc were recorded throughout the duration of the study to show the seasonal progression of vegetation growth, and in the case of photography, the expansion of cover relative to soil proportions, which reflect more strongly in the red wavelengths. To identify variation in phenology represented by vegetation height and gcc, the median and Interquartile Range (IQR) of all measurements in the moist and dry sites were compiled.

Figure 3.5 Photographs of plot 2c in the moist study site taken from a digital camera mounted on a metal frame. Photos capture temporal changes in vegetation structure and are used to calculate vegetation indices.

To determine moisture variability and soil characteristics within and between sites following the Kenow Wildland Fire, soil cores were extracted adjacent to vegetation plots, and oven-dried at 105° C for 24 hours based on the methods established by Carter & Gregorich (2008). The dry soil weight and volume of the soil sample were used to calculate bulk density which provides an understanding of soil porosity and compaction (Carter & Gregorich, 2008). Soil bulk density depth increments were compared with plot measurements including vegetation height, VWC, lodgepole pine seedling density, and gcc to identify any correlation with soil bulk density.

To assess variations in biomass and carbon accumulation between the two sites, regenerating herbaceous biomass harvested in 2019 (Figure 2.6) was air-dried for ten months before being weighed. Given that harvested vegetation was primarily herbaceous, with stem thickness of no more than 3 cm, further drying was not required after ten months. Biomass harvested in 2020 and 2021 was oven dried at 60° C until the weight of the biomass no longer fluctuated (approximately 48 hours). The carbon content of herbaceous vegetation was assumed to be 47.5 % of dry biomass weight based on Zehetgruber et al. (2017).

Figure 3.6 A biomass plot harvested in September 2019, from the moist site. The image on the left shows the plot prior to harvest, while the image on the right is post-harvest.

3.3.2 RPAS image data processing

To remove image distortion, displacement, and ensure image features are in the correct position, the RPAS imagery collected in 2018 was orthorectified to a 2018 LiDAR-derived Digital Surface Model (DSM). Orthorectification results in an image that accurately represents the Earth’s surface and facilitates measurements within and between images. To orthorectify the images, ArcGIS Pro georeferencing was used to establish ground control points between RPAS imagery and LiDAR surfaces using objects such as tree stumps, boulders, and trees that were identifiable in both datasets. Due to increased vegetation cover that raised the difficulty in matching LiDAR and RPAS features, RPAS images from 2019 and 2021 were georeferenced to the 2018 RPAS image. The number of ground control points ranged from 14 to 22 and all images were transformed using a 2^{nd}-order polynomial transformation. Total Root-Mean-Square Error (RMSE) for each image ranged from 0.07 to 0.21 and images were visually compared to ensure alignment of identifiable features such as the eddy covariance tower, walking trails, and notable terrain features.

RPAS images were split into individual RGB bands and used to calculate gcc (Equation 2.1). The minimum, mean, maximum, and standard deviation of RPAS gcc were extracted from each vegetation plot and compared with gcc values collected in the field. To model biomass quantities, RPAS gcc was calculated for each biomass plot and compared with field measured biomass. Scaling biomass from the plot-level to an RPAS gcc-based model of biomass provides an opportunity to compare annual changes in biomass and differences between study sites representing moisture endmembers.

To compare RPAS vegetation height with field measured vegetation heights, RPAS SfM point cloud data coincident with field measurements were outputted from Pix4Dmapper (Pix4D, Switzerland) and then processed in TerraScan (TerraSolid, Finland) to remove outlying points not representative of vegetation or the ground surface. RPAS point clouds were manually shifted and aligned with LiDAR point clouds using QT Modeller (Applied Imagery, United States) to ensure the continuity of z-values within the point clouds. To limit the influence of potential distortion in the point cloud, vegetation height was measured from the bottom of the point cloud to the mean of the maximum vegetation height in each plot. Plots located at the edges of the RPAS point clouds were removed to limit edge effects and minimize the influence of distortion.

3.3.3 Statistical methods and models

To compare multitemporal data and data between sites Shapiro-Wilk and Kolmogorov-Smirnov tests of normality were used in SPSS (IBM, United States) to determine the distribution of each dataset. To determine if a significant difference occurred between normally distributed data a two-sample t-test with unknown variance was used. While the Wilcoxon sign-rank test was used for non-normal data. In both cases, a 95 % confidence interval was used to determine significance. To identify the relationship between variables such as vegetation height and estimated RPAS or LiDAR height, linear regression was used in SPSS. Two-way ANOVA was used to determine the influence of study site location and time post-fire on mean vegetation height, gcc, and lodgepole pine seedling density at the peak of the growing season in 2019, 2020, and 2021. During the 2020 growing season, two-way ANOVA was used to determine if field-measured VWC and study site location had a significant influence on vegetation height and gcc. To complete this analysis, VWC was classified as low, low-medium, medium-high, and high based on their respective quantiles.

3.4 RESULTS

3.4.1 Influence of interannual climate variability on vegetation growth

Analysis of local climate at the moist site between the 2019 and 2021 growing seasons (May to September), summarized in Table 2.2, indicates that air temperature did not vary significantly between 2019 and 2020 or from 2020 to 2021 (t-test; $p = 0.30$; 0.11, respectively). Mean daily air temperature from May to September 2019 was 10.6° C, increasing to 11.1° C in 2020, and again to 11.9° C in 2021.

Table 3.2 Climate data collected over the course of this study. Precipitation data were collected at the moist site using a Geonor totalizing rain gauge. Temperature, snow depth, and SWE data are from the Akamina 2 climate station located near Cameron Lake (Agriculture and Irrigation, ACIS., 2021). Growing season is assumed to be from May 1st to September 30th of each year.

Year	Annual cumulative precipitation (mm)	Annual average temperature (° C)	Growing season cumulative precipitation (mm)	Growing season average temperature (° C)	Maximum SWE (mm)	Maximum snow depth (cm)
2018-2019	858	1.4	434	10.6	296	137
2019-2020	910	1.9	328	11.1	715	199
2020-2021	866	2.9	307	11.9	463	143

Daily precipitation did not vary significantly between 2019 and 2020 (t-test; p = 0.28) during the growing season, though it declined each year as average air temperatures increased over the study period. Despite drier summer season conditions in 2020, annual cumulative precipitation was greater in 2020 (910 mm) compared to 2019 (858 mm). Annual cumulative precipitation in 2021 was 866 mm, however, only 307 mm fell during the growing season, making it the driest summer of the study (Table 2.2). Growing season precipitation in 2021 varied monthly where June received 145 mm and July only received 3.9 mm. Cumulative precipitation in the Cameron Valley from 2019 to 2021 was below the average cumulative precipitation over the last 33 years (1380 mm) (Current and Historical Alberta Weather Station Data Viewer, 2022)

Snow depth, SWE, and timing of snowmelt are critical for the establishment of vegetation. Snow surveys conducted by Alberta Environment and Parks and Akamina climate station data indicated that the water year of 2019-2020 had the greatest snow depth (199 cm), 2018-2019 had the lowest snow depth (137 cm), and 2020-2021 had moderate snow depth in comparison (143 cm) (Table 2.2). Timing of the snow-free period varied each year with the earliest commencing on

May 30th, 2019; The 2020 snow-free period began 7 days later (June 6th); and was slightly earlier (June 2nd) in 2021.

Over decades, at the Waterton Park Gate, within about 18 km of the site, a comparison of water year precipitation and the 26-year average precipitation indicates that all years of this study received below the 26-year average precipitation (Figure 2.7). Moisture deficits were greatest in the summer of 2020 when precipitation was 183 mm below the average. The summer of 2018 was closest to the average with a precipitation deficit of 47 mm over the water year. Growing season temperature varied annually compared to the 46-year average (Figure 2.7). The growing season temperature was 0.3° C above the average in 2018, 0.6° C above the average in 2020, and 1.4° C above the average in 2021. The growing season in 2019 was an exception in this study as it was 0.5° C below the average temperature for the Waterton region.

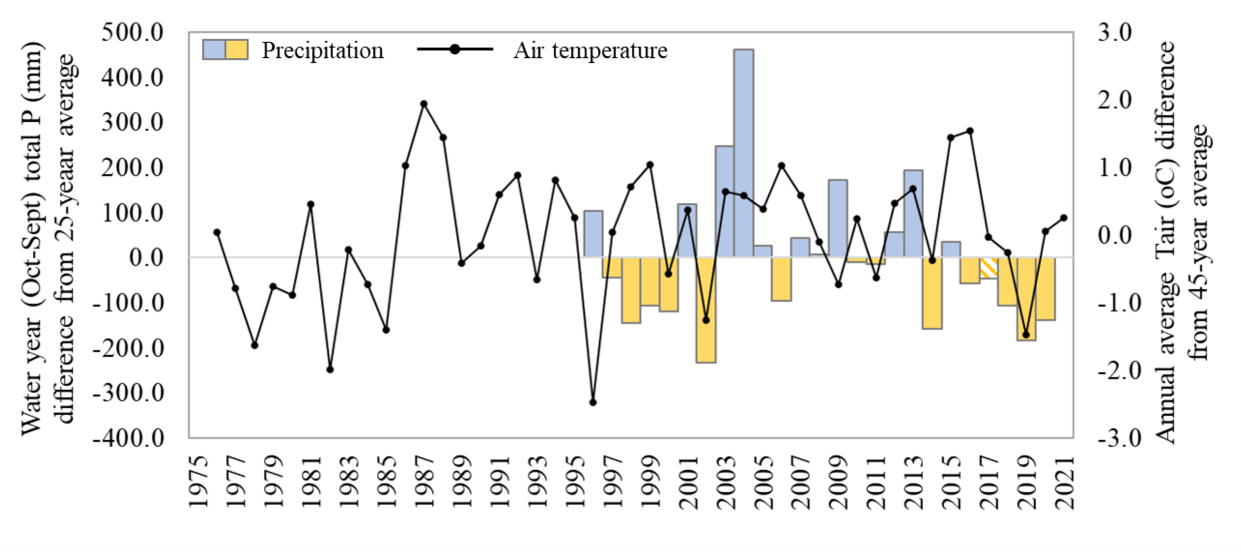

Figure 3.7 Water year precipitation deviation from the 26-year average and temperature deviation from the 46-year average at the Waterton Park Gate. Yellow bars represent below average precipitation while blue represents above average precipitation. The dashed orange bar represents the year of the Kenow wildfire (2017) and shows the half decade period of below average precipitation at, and since, the Kenow wildfire.

3.4.2 Species composition variation with time since fire

In the first-year post-fire, regenerating vegetation was comprised of short herbaceous species with high proportions of exposed ground (51 %) and coarse woody debris (10 %) determined from plot photography (Table 2.3). Herbaceous vegetation was still dominant in 2020, however, woody vegetation had established in small proportions (2 %). Vegetation cover expanded over the first three years post-fire, reducing the proportion of exposed ground to 7 % and coarse woody debris to 0.2 % of the total cover. In contrast, the dry site contained a larger proportion of seedlings with fireweed being the dominant species. Herbaceous vegetation in the dry site was composed of forbs, with no graminoid species identified, while the moist site was composed of a mix of forbs (63 %) and graminoid (31 %). Species richness in the moist site decreased from 2018 where 34 species were present (21 identified and 13 unidentified) to 24 species (17 species identified and seven unidentified) in 2020. In the dry site, only nine species were identified in 2020, revealing much lower species richness compared to the moist site.

Table 3.3 Total ground cover (%) for the moist site in 2018 and 2020, and the dry site in 2020. Values represent the average percent ground cover ± the standard error.

Latin Name	**Moist site 2018 (n = 17 plots)**	**Moist site 2020 (n =31 plots)**	**Dry site 2020 (n =2 9 plots)**
Chamaenerion angustifolium	6 ± 7	22 ± 5	40 ± 5
Chrysopsis villosa	0 ± 1	4 ± 1	2 ± 1
Elymus glaucus	0 ± 2	5 ± 2	0 ± 2
Phleum pratense	0 ± 0	0 ± 0	0 ± 0
Xewrophyllim tenax	4 ± 3	3 ± 2	3 ± 2
Spiraea beulifolia	1 ± 1	2 ± 1	1 ± 1
Robus parviflorus	4 ± 5	19 ± 4	3 ± 4
Veratrum viride	0 ± 2	4 ± 1	0 ± 1
Poe pratensis	0 ± 4	18 ± 3	0 ± 3
Vicia sativa	0 ± 0	0 ± 0	0 ± 0
Heracleum sphondylium	0 ± 0	0 ± 0	0 ± 0
Erythranthe lewisii	0 ± 2	3 ± 2	0 ± 2
Pinus contorta	0 ± 0	0 ± 0	1 ± 0

Camagrotis montanensis	1 ± 0	0 ± 0	0 ± 0
Bouteloua curtipendula	6 ± 1	0 ± 1	0 ± 1
Lallemantia iberica	2 ± 1	0 ± 0	0 ± 0
Geranium nicknelii	7 ± 1	0 ± 1	0 ± 1
Equisetum arvense	2 ± 1	1 ± 0	0 ± 0
Arnica cordifolia	3 ± 1	0 ± 1	0 ± 1
Vaccinium myrtillus	0 ± 0	0 ± 0	0 ± 0
Fragaria vesca	0 ± 0	0 ± 0	0 ± 0
Thalictrum venulosum	0 ± 0	0 ± 0	0 ± 0
Cirsium foliosum	0 ± 0	0 ± 0	0 ± 0
Lonicera capifolium	0 ± 0	0 ± 0	0 ± 0
Unknown species	3 ± 3	10 ± 2	1 ± 2
Moss	0 ± 3	0 ± 2	15 ± 3
Bare Ground	51 ± 6	7 ± 5	25 ± 5
Debris	10 ± 2	0 ± 2	8 ± 2

In the summer of 2020, lodgepole pine seedling counts ranged from 0-2 seedlings per plot (average = 0.21 seedlings m^{-2}, SD = 0.44) in the moist site and 0-16 seedlings per plot (average = 3.4 seedlings m^{-2}, SD = 3.54) in the dry site. In total, nine seedlings were counted in the moist site, while 142 were counted in the dry site. Lodgepole pine density was negatively impacted by hot, dry growing conditions in 2021, where a total of four seedlings (average = 0.08 seedlings m^{-2}, SD = 0.28) were counted in the moist site and 124 (average = 3.0 seedlings m^{-2}, SD = 3.46) were counted in the dry site. The reduction in seedling counts could indicate that conifer seedlings are impacted by warmer, drier conditions associated with climate change. A comparison of seedling counts within vegetation plots indicated that seedlings had a significantly negative correlation with VWC (Kendall's tau-b = -0.37, p = 0.001, n = 48) and gcc (Kendall's tau-b = -0.35, p = 0.001, n = 52), but had a positive correlation with gcc standard deviation (Kendall's tau-b = 0.25, p = 0.019, n = 52) and bulk density at the 5-10 cm depth (Kendall's tau-b = 0.24, p = 0.031, n = 49). The difference in seedling quantities was significantly different between the moist and dry sites (H = 24.5, p < 0.001).

3.4.3 Do moist montane valley sites enhance the rate of herbaceous vegetation recovery compared to drier sites?

A summary of measured vegetation characteristics, including height, cover, gcc, and biomass between the moist and dry sites and statistical comparisons between the two sites are shown in Table 2.4. Vegetation height and gcc were significantly greater in the moist site compared to the dry site (Table 2.4). In 2020, moist site vegetation was, on average, 0.30 m taller (t-test, $p < 0.001$), while gcc was 0.08 greater (t-test, $p < 0.001$) than the dry site. In 2021, vegetation heights increased at the moist site, though differences were slightly less than in 2020. In 2021, moist site vegetation was on average 0.26 m taller (Wilcoxon, $p = 0.05$) and gcc was 0.08 (Wilcoxon, $p = 0.005$) greater than the dry site.

Despite average differences between sites, vegetation phenology also varied from year to year between the moist and dry sites, and with variability in air temperature and moisture availability (Table 2.4). In the first year of the study, moist site gcc index increased significantly from 2018 to 2019 by 0.05 (Wilcoxon, $p < 0.001$), while cover expansion slowed as short herbaceous ground cover vegetation filled in openings between plants between 2019 and 2020 (Wilcoxon, $p = 0.04$). By 2020, when both sites were measured, peak vegetation height in the moist site occurred during the first week of August (Figure 2.8), while the dry study site reached peak vegetation height approximately 12 days later than the moist site. Peak gcc occurred two to three weeks earlier in the moist site, indicating that vegetation cover increases earlier in the season before vegetation reaching maximum height (Figure 2.8). Within the dry site, gcc was relatively consistent in 2020 and 2021.

Table 3.4 Comparison of vegetation and soil attributes between the moist and dry site over the 2020 field season, including the difference and significance of difference.

	Vegetation cover (intercept)		gcc		Volumetric water content (%)		Soil bulk density average of all depths (g cm^{-3})		Biomass (g m^{-2})	
	Dry site	Moist site	Dry site	Moist site	Dry site	Moist site	Dry site	Moist site	Dry site	Moist site
Mean	1.12	2.61	0.37	0.45	7.68	13.9	0.76	0.75	269	296
Standard deviation	0.55	0.92	0.03	0.04	4.73	10.3	0.17	0.14	66.9	217
Difference relative to the moist site (±)	1.49		0.08		6.18		-0.02		27	
Sig. of change	<0.001		<0.001		<0.001		0.99		0.83	

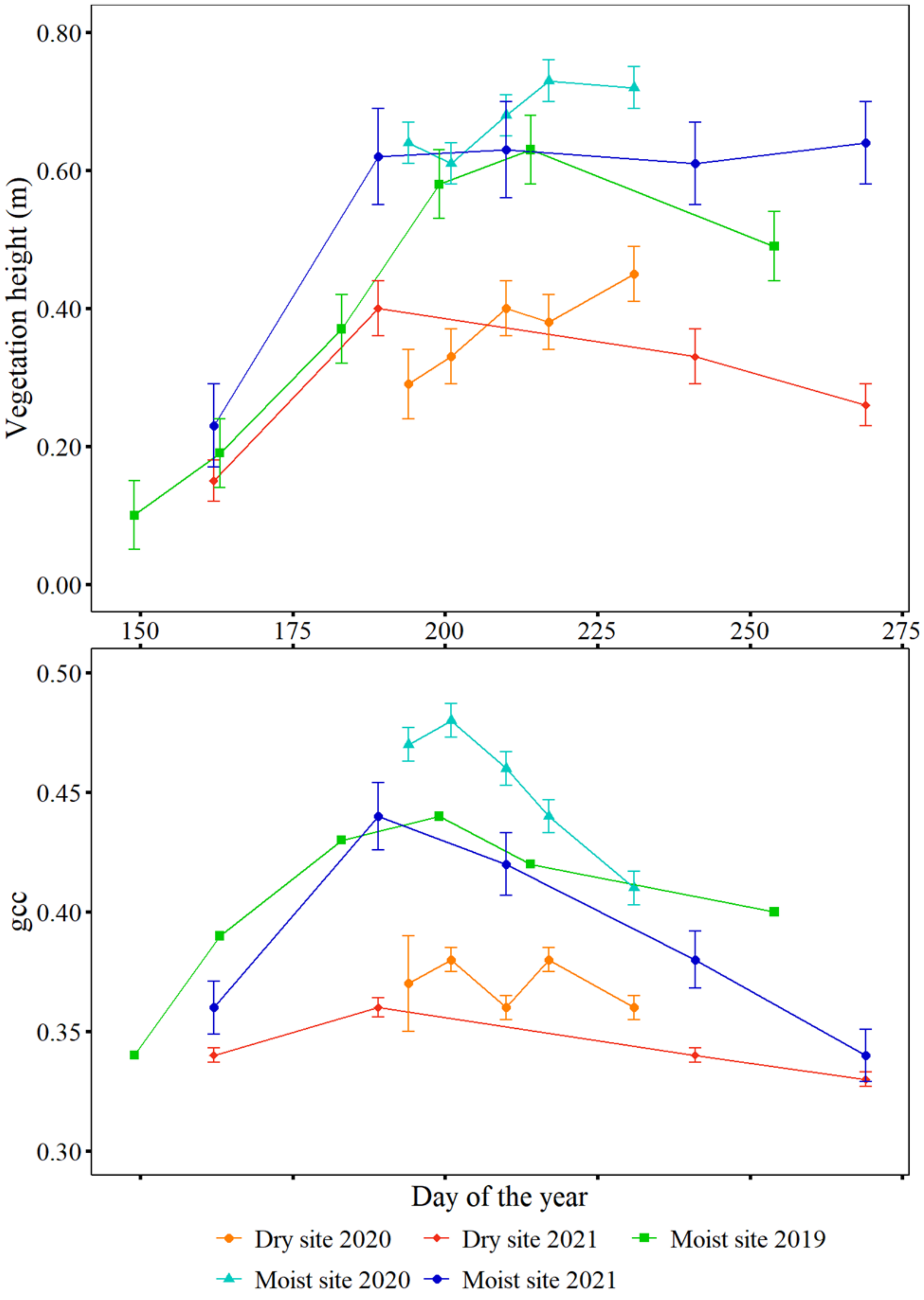

Figure 3.8 Annual changes in vegetation height and gcc from 2019 to 2021 in the moist and dry site. Data collection for the dry site began in the summer of 2020, therefore no data are available for this site in 2019.

Following abnormally hot, dry conditions in 2020 and 2021 (Figure 2.7), vegetation height (average change from 2019 = - 0.10 m; Wilcoxon, p = 0.11) and gcc (average change = -0.02; Wilcoxon, p = 0.07) decreased during this period at the moist site (Figure 2.8). Changes in height between years were smaller and not significant in the dry site (average change = -0.07 m, paired t-test p = 0.35), while gcc differences were greater (average change = -0.02; Wilcoxon, p = 0.03).

Table 3.5 Bulk density data collected in the moist site and dry site on September 16th and 20th, 2020. Values represent the average bulk density with the standard error and n value below. The combined sites is the average of all samples from the moist and dry site with the standard deviation and N below.

	Bulk density ($g\ cm^{-3}$), 0-5 cm	Bulk density ($g\ cm^{-3}$), 5-10 cm	Bulk density ($g\ cm^{-3}$), 10-15 cm	Average bulk density ($g\ cm^{-3}$), all depths
Moist site	0.61 (SE ± 0.03, n = 30)	0.75 (SE ± 0.04, n = 30)	0.94 (SE ± 0.04, n = 24)	0.75 (SE ± 0.03, n = 22)
Dry site	0.55 (SE ± 0.05, n = 22)	0.91 (SE ± 0.05, n = 19)	0.98 (SE ± 0.06, n = 13)	0.76 (SE ± 0.04, n = 29)
Combined sites	0.58 (SD ± 0.20, N = 52)	0.81 (SD ± 0.22, N = 49)	0.95 (SD ± 0.21, N = 37)	0.75 (SD ± 0.16, N = 51)

The average bulk density for all plots in this study were 0.58 $g\ cm^{-3}$ (SD = 0.20, n = 52) at the 0-5 cm depth, 0.81 $g\ cm^{-3}$ (SD = 0.22, n = 49) at the 5-10 cm depth and 0.95 $g\ cm^{-3}$ (SD = 0.21, n = 37) at the 10-15cm depth (Table 2.5). Average bulk density at the 5-10 cm depth was significantly (H = 3.93, p = 0.048) different between the moist (0.75 $g\ cm^{-3}$) and dry site (0.91 $g\ cm^{-3}$). However, the 0-5 cm, 10-15 cm, and average of all depths was not significantly different between sites (Table 2.5). A comparison of bulk density samples, regardless of site, and vegetation metrics indicated that bulk density did not have a significant correlation with vegetation growth except for a weak, but significant correlation with seedling counts (Kendall’s tau-b = 0.24, p =

0.31). However, in the dry site, vegetation height and bulk density at the 10-15 cm depth were significantly correlated ($R^2 = 0.40$, $p = 0.02$, $n = 13$) indicating that vegetation height was generally greater in plots with a higher 10-15 cm depth bulk density.

Two-way ANOVA was used to estimate changes in mean vegetation height, gcc, and lodgepole pine seedling density based on site location and year. It was found that there was no significant interaction between the effects of site location and year on vegetation height (F (2, 120) = 0.23, p = 0.64). Analysis of the individual effects showed that the influence of site location had a greater significance ($p < 0.001$) than year ($p = 0.47$) on mean vegetation height. Similarly, the interaction of site location and year had no significant influence on lodgepole pine seedling density (F (1, 102) = 0.05, p = 0.82). However, analysis of the individual effects showed that site location had a greater impact ($p < 0.001$) than year ($p = 0.70$) on lodgepole pine seedling density. In contrast, the interaction of site location and year had a significant impact on mean gcc (F (1, 120) = 10.32, p = 0.002).

Table 3.6 Biomass accumulation in the moist and dry sites from 2019 to 2021 in g m^{-2}.

	Moist site 2019	Moist site 2020	Moist site 2021	Dry site 2020	Dry site 2021
Mean	335	296	298	269	117
Standard Deviation	103	217	197	67	45
n	11	4	6	4	6

While height and cover are easily measured and compared between plots, biomass provides a more direct quantification of change related to differences in plant productivity. Biomass was greatest in the moist site in 2019 where the plot average was 335 g m^{-2} (Table 2.6; Figure 2.8). Biomass decreased by 37 g m^{-2} in the moist site from 2019 to 2021, but the reduction was not significant (Kruskal Wallis H = 0.68, p = 0.71). In the dry site, biomass was significantly (F (1,8)

= 18.72, p = 0.003) greater in 2020 than in 2021 (Table 2.6; Figure 2.9). Despite the increased biomass accumulation in the moist site compared to the dry site, there were no significant (F (1,18) = 3.08, p = 0.10) differences between the two sites over the course of this study. Reductions in biomass from 2019 to 2021 correspond with high air temperatures (~1.5° C warmer than the long-term record at Waterton Gate) and low growing season precipitation (Table 2.2; Figure 2.7).

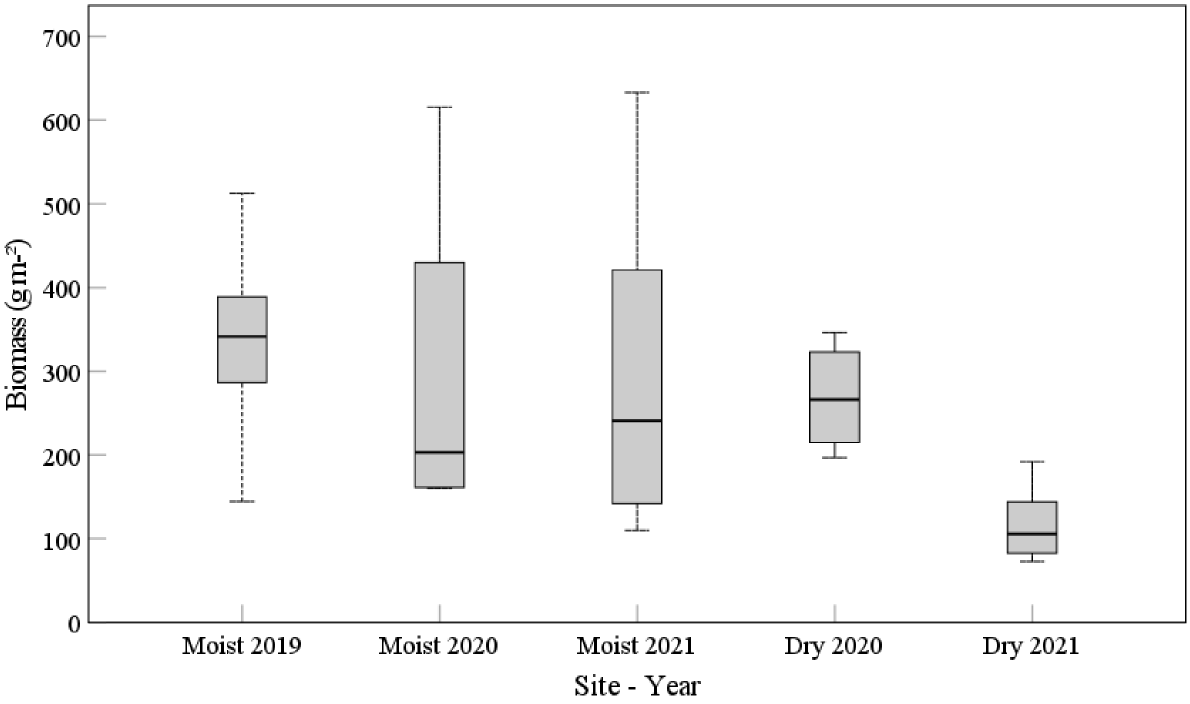

Figure 3.9 Biomass in the moist site from 2019 to 2021 and the dry site in 2020 and 2021. Boxes represent the 1st quartile, median, and 3rd quartile.

3.4.4 Using RPAS optical imagery and SfM photogrammetry for capturing variability in post-fire vegetation regeneration

The utility of using RPAS SfM for quantifying changes in post-fire vegetation height requires field measurements as a source of validation. As vegetation grows taller, it is expected that the ability to differentiate between vegetation heights from the ground surface will improve. However, the correlation between RPAS SfM vegetation height and field-measured vegetation height in the moist site only increased slightly from 2019 ($R^2 = 0.07$, p = 0.32) to 2021 ($R^2 = 0.08$, p = 0.37). RPAS best captured the variability of vegetation height in the dry site, 2021 ($R^2 = 0.83$, $p < 0.001$), where the average measured vegetation was 0.05 m greater than field measured vegetation. The inclusion of all years and sites improved the correlation between RPAS and field measured vegetation height ($R^2 = 0.54$, $p < 0.001$) (Figure 2.10). However, RPAS SfM modelled height did not correlate with biomass ($R^2 = 0.0007$, $p = 0.129$) (Figure 2.10).

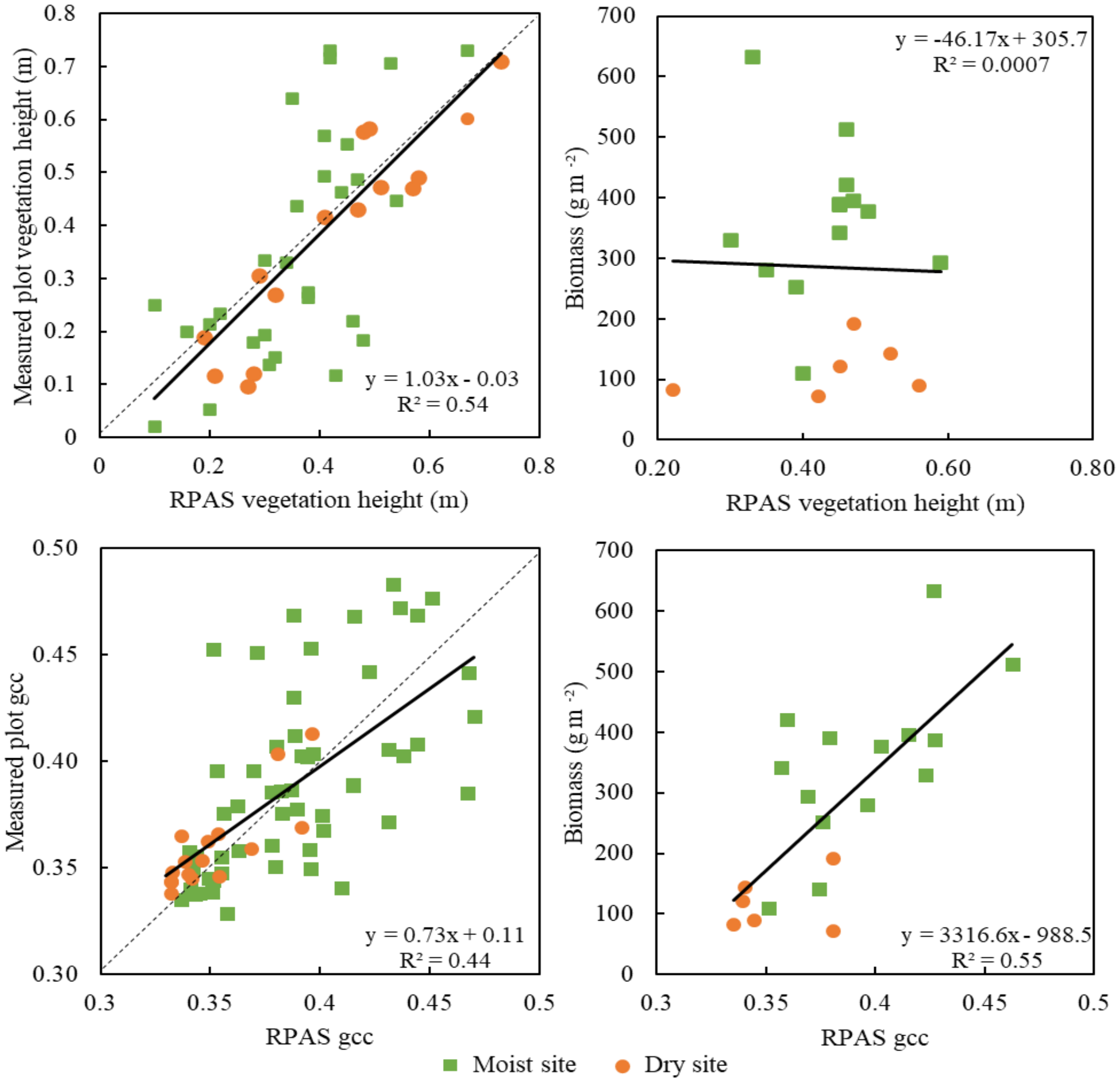

Figure 3.10 Linear regression between RPAS vegetation metrics and field measurements. RPAS-modelled vegetation height had a significant correlation with field-measured vegetation height ($p < 0.001$) but not with biomass ($p = 0.129$). RPAS-modelled gcc had significant correlations with field-measured gcc ($p < 0.001$) and biomass ($p = 0.002$).

RPAS gcc had a significant correlation with field measured gcc ($R^2 = 0.44$, $p < 0.001$) and had a difference in the mean of 0.003. RPAS gcc also had a significant correlation with biomass ($R^2 = 0.55$, $p = 0.002$), indicating that optical RPAS imagery may provide a more effective way to model plot-level vegetation attributes than SfM point clouds during the early stages of regeneration (Figure 2.10).

3.5 DISCUSSION

3.5.1 Climatology of the Cameron Valley in the early post-fire years

Climate is a key driver of herbaceous vegetation growth, and the establishment and survival of conifer seedlings (Andrus et al., 2018; Busby et al., 2020; Dodson et al., 2013; Rother, 2015). Conditions over the course of this study fall below the long-term mean water year precipitation and above the long-term growing season temperature (Table 2.2). Harvested biomass in 2019 was greatest over the course of the study and was also the only year cooler than the 45-year average growing season temperature (Table 2.6; Figure 2.7). Reductions in biomass from 2020 to 2021 within the dry site (and slight increase in the moist site) may be due to changes in seasonal climate conditions. From the 2020 to 2021 growing season, precipitation was reduced and temperature increased, which corresponded with an earlier peak in vegetation height in 2021 (Figure 2.8), overall reduced vegetation height, gcc, and biomass (Table 2.6), and reduced lodgepole pine seedling counts at both moist and dry sites. The reduction in lodgepole pine seedling counts aligns with research by Rother et al. (2015) who determined that warming temperatures could limit the establishment and survival of conifer seedlings regardless of the amount of precipitation.

Waterton has experienced above average temperatures in nine of the last ten years, and below average precipitation in seven of the last ten years (Figure 2.7). If these climate trends continue, it may be expected that regeneration will be reduced or lag in comparison to what may be expected under average regional climate conditions. Shade-tolerant species such as spruce and fir may be more intolerant to increasing temperatures and reduced precipitation, driving lags in establishment, and creating an advantage for species such as lodgepole pine and aspen (Busby et al., 2020).

3.5.2 Do moist montane valley sites enhance the rate of herbaceous vegetation recovery compared to drier sites?

The results of this chapter indicate that the moist riparian site experienced enhanced herbaceous vegetation accumulation compared to the dry site, determined by field measured species richness, vegetation height, and gcc (Table 2.3; Figure 2.7). The moist site contained a greater proportion of forbs and graminoid species within the first two years post-fire and a lower proportion of exposed ground compared with the dry site. The influence of moisture on species composition has also been observed in the Klamath-Siskiyou Mountains of Oregon, where moist sites experienced higher proportions of forbs compared to drier areas, which were more favourable to hardwoods and shrubs (Donato et al., 2009). Differences in the proportion of woody vs. herbaceous vegetation in the initial years post-fire may shape the future forest composition by increasing competition and altering the suitability for the establishment of shade-tolerant and shade-intolerant species (Bonnet et al., 2005; Gendreau-Berthiaume et al., 2018).

Here, inter-, and intra-annual peak vegetation height increased from 2019 to 2020 but declined in 2021 (Figure 2.8). These results indicate that moisture availability could be a limiting factor for the accumulation of herbaceous vegetation within the valley, with the moist site experiencing significantly greater VWC than the dry site (t-test; $p < 0.001$). However, the opposite was found regarding the establishment of conifers, where lodgepole pine densities were the greatest within the dry site, though no significant relationship was found between vegetation height and VWC at the plot level (t-test; $p = 0.10$). Decreased vegetation height and gcc from 2020 to 2021 in both the moist and dry sites was likely due to an anomalously warm, dry summer and reduced snow accumulation in the months prior. This indicates that both herbaceous vegetation and lodgepole pine establishment are sensitive to climatic stress, in this case, a lengthy period of four years of drier than normal conditions and abnormally warm growing seasons.

The summer of 2021 was the driest of the study (Figure 2.7), the second driest in 25 years, and the second warmest year in 45 years, following an extended dry period (Figure 2.7). Irregular precipitation from early onset of snowmelt and over the growing season corresponds with reduced growth of herbaceous vegetation, which appears to be sensitive to changes in moisture. Comparison of gcc between biomass plots and vegetation plots indicates that biomass may have been underrepresented in 2020, particularly in the moist site, meaning there was potentially an increase in biomass from 2019 to 2020, corresponding with vegetation growth measured in the vegetation plots. Decreased biomass from 2020 to 2021 reflects observed overall decreases in vegetation height and gcc observed in the vegetation plots (Figure 2.8; Figure 2.9).

Estimates of carbon loss from the Kenow Wildland Fire by Gerrand et al. (2021) suggest that an average of approximately 11 kg C m^{-2} was lost from the moist study site, ~8.6 kg C m^{-2} was lost from the dry study site, and 10 kg C m^{-2} was lost from the combined sites due to tree combustion. Regenerating vegetation in the first four years post-fire accounts for 2.6 %, 1.3 %, and 2.0 % of the carbon lost in the moist site, dry site, and combined sites in 2021. Although regeneration in the Cameron Valley is a small proportion of the biomass lost, the growth of herbaceous vegetation has been rapid. The accumulation of 250 g C m^{-2} of biomass by year four approaches that accumulated after 11 years at Yellowstone National Park (340 g C m^{-2} aboveground biomass) and after nine years of sagebrush accumulation (210 g C m^{-2}) in Southern

Idaho (Fellows et al., 2018; Turner et al., 2016). However, as this is mostly herbaceous (especially in the moist site), the majority of biomass accumulated as Gross Primary Productivity (GPP) senesces in autumn and eventually decomposes over winter and into the following spring, suggesting that the ecosystem is not yet an annual carbon sink.

3.5.3 Post-fire conifer establishment within moist vs. dry sites

In both 2020 and 2021, all conifer seedlings identified were lodgepole pine, a serotinous species that is capable of rapid post-fire establishment. Results indicate that lodgepole pine quantities in the valley bottom range from 1,200 seedlings ha^{-1} to 34,000 seedlings ha^{-1} in 2020 and 800 seedlings ha^{-1} to 30,000 seedlings ha^{-1} in 2021. Observed yellowing or loss of needles, seedling mortality, and reduced lodgepole pine densities within the vegetation plots may be associated with the hot, dry conditions experienced in 2021. Lodgepole pine densities in the Cameron Valley compared with minimum densities from pine dominated regions such as Yellowstone National Park, where mean lodgepole pine densities ranged from an average of 29,381 to 60,000 stems ha^{-1}, indicate low rates of post-fire establishment (Turner et al., 1997; Turner et al., 2004).

A more regionally representative comparison would be with Glacier National Park where 33,067 stems ha^{-1} were present six years post-fire. (Harvey et al., 2016). According to Harvey et al. (2016), lodgepole pine establishment pulsed one-year post-fire and continued for three to five years. Timing of peak establishment for all conifers varied between Glacier National Park, six years post-fire, and Yellowstone National Park, 12 years post-fire (Harvey et al., 2016). These findings indicate that four years after the Kenow Wildland Fire, lodgepole pine establishment in the Cameron Valley may be near its peak, especially if current dry conditions continue in the coming years.

The density and distribution of lodgepole pine seedlings within the moist and dry sites are influenced by the pre-fire tree distribution. Research by Gerrand et al. (2020) identified 72 burnt lodgepole pine trees within three tree plots (400 m^{-2}) in the dry site and 21 lodgepole pine trees within three tree plots in the moist site. The greater number of lodgepole pines within the dry site increases the seed availability for rapid post-fire establishment. Additionally, the negative correlation between VWC and lodgepole pine seedlings indicates that drier conditions may be more suitable for establishment in this region at this time. However, future drying beyond what is currently observed may have a negative influence on the establishment of lodgepole pine seedlings. The positive correlation between gcc standard deviation and lodgepole pine seedlings may indicate that competition for light and nutrients is limiting lodgepole pine seedling establishment, resulting in more seedlings establishing in areas of patchy vegetation cover. In the coming years, establishment may shift to non-serotinous species such as white and Engelmann spruce, and sub-alpine fir which were present in the Cameron Valley before the Kenow Wildland Fire (Gerrand et al., 2021). Unlike lodgepole pine, spruce and fir species rely on wind to disperse seeds from the live tree edge, often resulting in delayed establishment compared to serotinous species (Donato et al., 2009).

3.5.4 Using RPAS optical imagery and SfM photogrammetry for capturing variability in post-fire vegetation regeneration

Numerous studies have illustrated the efficacy of SfM point clouds for capturing environmental structure, including vegetation height (Goodbody et al., 2017; Goodbody et al., 2018; Nuijten et al., 2019). This study found that the correlation between SfM and field measured vegetation height was significant when all years were considered ($R^2 = 0.54$, t-test; $p < 0.001$), but tended to overestimate field-measured vegetation heights < 0.5 m in height and under-estimated vegetation heights > 0.5 m (Figure 2.10), apart from the moist site in 2021. Potential limitations of SfM point clouds in this study include the high cover and density of herbaceous vegetation, the presence of necromass within the regenerating vegetation, and the lack of ground control points to remove the distortion within RPAS SfM point clouds. Previous research by Goodbody et al. (2018) has shown the efficacy of SfM for identifying short (~0.5 m) conifer seedlings with low stand density and cover. In this study, mean vegetation height at the plot level was shorter (average of 0.34 m) than the trees identified by Goodbody et al. (2018). Additionally, short, dense herbaceous cover may reduce the ability of SfM point clouds to capture variation in vegetation height.

The post-fire landscape includes snags, burnt logs, and burnt roots that can be at or below the height of regenerating vegetation. Without separating necromass from biomass in the processing methods, bias will exist as not all points are representative of regenerating vegetation. The high point density of SfM data ensures both necromass and biomass will be sampled, and confusion between the two will be exacerbated for short-lived vegetation and during the early stages of regeneration.

3.6 CONCLUSION

This study examined the recovery of post-fire vegetation growth in a moist and dry montane site, during the initial four years post-fire, a period that was abnormally warm and dry. This chapter then examined the utility of RPAS optical indices and SfM point clouds for tracking spatiotemporal variability in change over three years. In the early years following a severe montane wildland fire, herbaceous vegetation regeneration was significantly greater in the moist site compared to the dry site. However, lodgepole pine seedling growth was more prolific in the dry site, counter to the understanding that moist conditions relate to increased conifer establishment. As expected, both sites experienced significant declines in herbaceous vegetation from 2020 to

2021 following severe hot and dry conditions. Although not to the same degree, conifer seedlings were also sensitive to abnormally warm years, and prolonged drying could reduce conifer regeneration within Waterton. Although regeneration has been rapid, this initial post-fire forest holds only a small portion (~ 2 %) of carbon lost in the Kenow Wildland Fire.

Vegetation monitoring following wildland fire in montane ecosystems can be difficult. RPAS SfM point clouds and optical vegetation indices proved to be effective methods of modelling vegetation structure in the initial years of regeneration. The ability to model biomass accumulation allows for predictions related to carbon storage and assessment of ecosystem health in this critical stage of ecosystem recovery. However, further research is required to understand how the efficacy of RPAS changes as post-fire ecosystems change through different stages of regeneration. Predictive live vegetation attribute models based on SfM point clouds are weaker in the earliest stages of regeneration or over drier, low-productivity sites due to confusion between living and dead biomass, and the short stature and cover of vegetation. In the initial stages of regeneration, optical approaches, such as gcc, prove to be more reliable, but as vegetation height and cover increase in the latter stages of regeneration, SfM approaches are expected to improve and become more reliable.

As the Cameron Valley recovers from the Kenow Wildland Fire, the ecosystem will continue to change as vegetation regenerates and progresses toward a healthy forest structure. Given the high annual precipitation in this ecosystem, the effects of climate change may not be as pronounced as in other montane regions, but the study has shown the impact annual variations in climatic conditions can have on vegetation. Montane regions with less annual precipitation may experience similar trends during periods of moisture stress, but potentially to a greater degree.

CHAPTER 3: SCALING EARLY POST-FIRE VEGETATION REGENERATION USING MULTISPECTRAL LIDAR

4.1 INTRODUCTION

Wildland fires are a necessary component of healthy ecosystem development. Fires create ecosystem conditions that promote new vegetation growth by removing organic matter from the forest floor, exposing mineral soils, increasing light availability, and returning nutrients to the soil (Landhäusser et al., 2010; Tautenhahn et al., 2016; Tepley & Veblen, 2015; Zehetgruber et al., 2017). However, anthropogenic climate change is altering wildland fire behaviour by increasing fire frequency, burn severity, and the proportion of area burned each season (Jolly et al., 2015; Kirchmeier-Young et al., 2017; Westerling, 2016). In Canada, there has been a 1.5 to 6 times increase in the likelihood of extreme wildland fire occurrence since 2010 (Kirchmeier-Young et al., 2017). Changing climate may also influence the development of future forest regimes, resulting in reduced tree density, species composition changes, and shifting tree establishment to higher elevations where more moisture is available (Donato et al., 2016; Tepley et al., 2017; Urza & Sibold, 2017).

While intermediate post-fire succession is well-understood, the early foundational years of post-fire succession and potential shifts in forest species regeneration are not as well known. Initial post-fire vegetation regeneration includes herbaceous vegetation and low shrubs which provide shelter for establishing conifer and deciduous seedlings (Tepley et al., 2014). The distribution and growth of early post-fire regeneration are influenced by burn severity, pre-fire forest composition, distance from seed sources, aspect, elevation, shade, moisture, climate, and competition with other species (Bonnet et al., 2005; Donato et al., 2009; Tepley et al., 2014). The development of mature forests is closely correlated with the composition and structure of early post-fire regeneration

(Turner et al., 2016). By understanding the topographic and environmental factors that influence early post-fire regeneration, land managers can build an understanding of forest trajectories.

To understand the impacts of moisture (Chapter 2) and environmental drivers of post-fire regeneration, there is a need to determine growth rates across broad areas that are difficult to access and require time to measure. Airborne remote sensing technologies such as Light Detection and Ranging (LiDAR) offer the ability to collect high-resolution data across complex montane landscapes. LiDAR emits laser pulses toward the ground surface creating a three-dimensional point cloud that represents vegetation structure (Lim et al., 2003). LiDAR provides information such as elevation, which can be used to derive other spatial characteristics of the land surface, including aspect, slope, and topographic position. Spatial characteristics are important indicators of moisture availability and can drive greater biomass accumulation in regions with low topographic position, at the toe slopes of montane valleys, and on north-northeastern aspects where moisture availability is typically higher (Swetnam et al., 2017). For example, Seidl et al. (2012) used LiDAR-based models to determine how variation in environmental drivers such as solar energy, soil physical properties (ability to store moisture), and precipitation influenced the spatial variation of aboveground biomass. Variation in environmental drivers representing moisture availability (solar radiation and soil capacity to retain moisture) had the greatest influence on the spatial distribution of aboveground biomass and accounted for 53.8 % of the spatial variation (Seidl et al., 2012).

There is a need to better understand the spatial variability of montane forest regeneration in the early years following severe wildland fires. While plot measurements can be used, montane ecosystems can be difficult to access, therefore, a scaled field and remote sensing approach for quantifying post-fire vegetation changes were implemented. The overall goal of this chapter is to develop a valley-scale model of biomass and identify the environmental factors that influence the spatial distribution of vegetation. The objectives of this study were to: (i) Assess the efficacy of airborne LiDAR canopy height models for capturing variability in post-fire vegetation structures (specifically height) in the first four years following a severe wildland fire. (ii) Use harvested plot biomass to develop a model of post-fire biomass change over a period of four years within the Cameron Valley, and (iii) Use the thematic information derived from airborne LiDAR within a machine learning framework to identify abiotic environmental factors that may influence biomass accumulation in a montane valley following severe wildland fire.

4.2 MATERIALS AND METHODS

4.2.1 Study area

This study was conducted within the most southerly part of the Canadian Rocky Mountains, in the Cameron Valley Waterton Lakes National Park (hereafter "Waterton") (113° 51' 42" W and 49° 5' 40" N) in Alberta, Canada (Figure 3.1 A). Waterton is located along the Rocky Mountain Continental Divide where the steep mountains (maximum elevation 2,900 m) drive orographic precipitation and temperature gradients, which reduce with distance from the divide. As such, the average annual cumulative precipitation is 1072 mm within the Waterton townsite, but areas near Cameron Lake, in the southern part of the park receive closer to 1380 mm annually, making Waterton the region with the highest precipitation in Alberta (Parks Canada, 2018a). Montane and subalpine ecoregions of Waterton are dominated by lodgepole pine (*Pinus contorta)*, sub-alpine fir (*Abies lasiocarpa)*, and Engelmann spruce (*Picea engelmannii)* (Parks Canada, 2018).

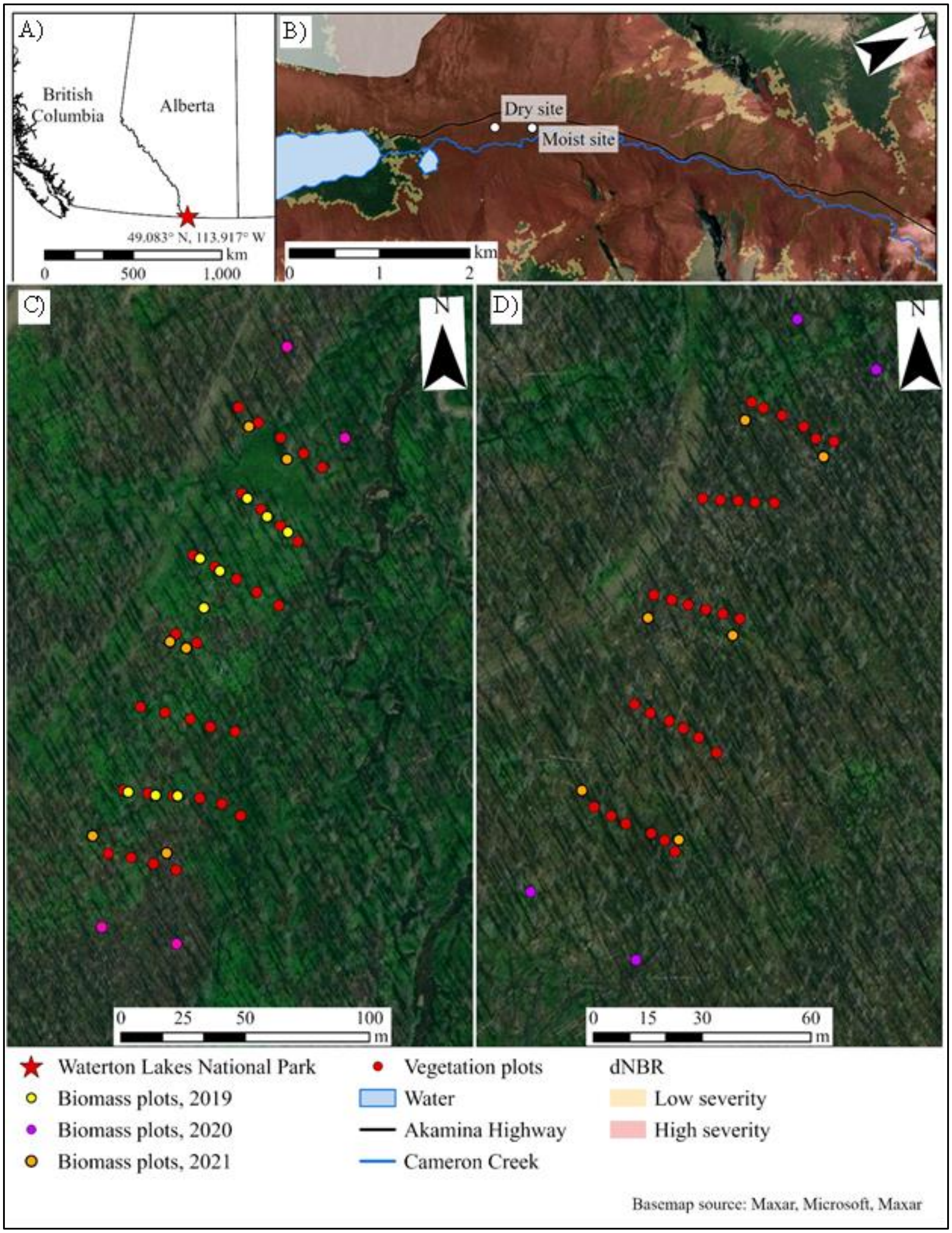

Basemap source: Maxar, Microsoft, Maxar

Figure 4.1) A) Location of Waterton within western Canada; B) location of two study sites and severity of the Kenow Wildland Fire shown as a Landsat OLI-derived differenced Normalised Burn Ratio (dNBR); C) The location of biomass and vegetation plots within the moist study site; D) The location of biomass and vegetation plots within the dry site, both of which are positioned over a basemap image from Earthstar Geographics.

On August 30, 2017, the Kenow Wildland Fire started from a lightning strike west of the Waterton boundary (Parks Canada, 2019). In the following weeks, warm temperatures and high winds drove the wildland fire through Waterton where it consumed 19,300 ha (38 %) of the National Park and 35,000 ha total (Parks Canada, 2019). Waterton has a history of fire suppression and no wildland fires have been observed in the Cameron Valley over the last century (Parks Canada, 2021). The combined high severity of the Kenow Wildland Fire and a history of fire suppression created an opportunity to quantify the impacts of the fire on post-fire regeneration in this montane environment.

Comparisons between measured vegetation structure within 60 microplots and multispectral LiDAR data were focused on two study sites located in the Cameron Valley. Sites were selected to represent moisture endmembers for vegetation growth (Figure 3.1 B, C, D) described in Chapter 2. The moist site (Figure 3.1 B, C) is located adjacent to Cameron Creek and contains intermittent streams running through the east side of the site, and smaller intermittent creeks flow through rills from the mountainsides into mid-summer. In the southern section of the site, there is an intermittent groundwater spring, which floods a portion of the site until late June when the snowpack at higher elevations has melted. The soil composition in the moist site is predominately silty in texture and organic with exposed mineral soils on the southern transects. The slope of the moist site ranges from 1° to 9° with an average of 4° (standard deviation (SD) ± 2°) and is east-facing. The average Volumetric Water Content (VWC), observed at 124 vegetation plots between July 12th and August 4th, 2020, was 15 % (SD ±11 %).

In July 2020, the dry site was established approximately 350 m south of the moist site to represent a dry region of the valley bottom (114° 2’ 27” W, 49° 1’ 51” N and 1656 m.a.s.l) (Figure 3.1B, D). The dry site is located approximately 175 m west of Cameron Creek and does not contain any sources of flowing water. Soil composition is predominately rocky, mineral soils with shallow organic layers in a flat region at the south end of the site. The slope in this site ranges from 1° to 13° with an average of 5° (SD ± 3°) and is east-facing. The average VWC between July 12th and August 4th, 2020, was 8 % (SD ± 5 %), making it significantly ($p < 0.001$) drier than the moist site.

4.2.2 Field Data Collection

Permanent vegetation plots within the moist and dry study sites were used to create a plot-based biomass model, described in detail in Chapter 2. Briefly, 31 permanent vegetation plots were established in the moist study site in 2018 with another 29 vegetation plots established in the dry study site in July 2020. Field data, including vegetation height, cover, and Green Chromatic Coordinate (gcc) from downwards-looking photography were collected approximately every 2-3 weeks throughout September 2018, summer 2019, 2020, and 2021. All plots were located using a Topcon Inc. (Canada) HiPer SR II survey-grade Global Navigation Satellite System (GNSS) with an accuracy of < 10 cm. In addition to vegetation measurements, photographs were taken of each plot using a digital camera (Nikon, Japan). Images were used to calculate the gcc of each plot (Nijland et al., 2014; Sonnentag et al., 2012). Gcc is the measure of greenness within an image and is used to track phenology and plant health (described in Chapter 2). To quantify biomass accumulation, within and between the moist and dry sites, biomass was harvested annually in 2019, 2020, and 2021 (described in Chapter 2). The location of each biomass plot was obtained using GNSS with < 10 cm accuracy. Vegetation was clipped at the ground surface and stored in large paper bags for processing (described in Chapter 2).

4.2.3 Multispectral and multi-temporal LiDAR data collection

To examine changes in biomass and environmental drivers of change, airborne LiDAR surveys were conducted on July 16, 2018, July 22, 2019, July 29, 2020, and July 16, 2021, using a Teledyne Optech Titan multispectral LiDAR system, flown on a fixed-wing Piper Navajo. The average flight height per survey was approximately 1200 m above the valley floor and each survey was flown with 50 % overlapping scanlines. LiDAR system parameterization and flight configuration are described in Table 3.1.

Table 4.1 Specification for airborne LiDAR flights. Point density is the average density of 10 randomly sampled locations in the Cameron Valley.

Year	Pulse repetition frequency (KHz)	Scan Frequency (Hz)	Scan Swath (deg)	Average Aircraft Speed (m/s)	Average Flying Altitude (m.a.s.l)	Average Point Density (Points m^{-2})
2018	100	40	38 ± 2	72	2879	9
2019	75	32	50	71	2603	7
2020	75	32	48 ± 2	73	2674	6
2021	75	32	48 ± 2	72	2670	7

4.3 DATA ANALYSIS

4.3.1 Vegetation plot data analysis

Field-measured vegetation at the time nearest each LiDAR survey were used to compare with LiDAR metrics (2018 - 2021) (described in Chapter 2), with plot locations illustrated in Figure 3.1. Briefly, vegetation height was determined by measuring the maximum vegetation height at the left, center, and right side of each plot using an extendable two-meter ruler. The mean of the maximum vegetation height and standard deviation were determined within each plot. Gcc, determined from down-looking photography, (described in Chapter 2) was used to estimate the proportion of exposed ground and green foliage. To account for tall vegetation with reduced density, gcc was multiplied by the mean of the maximum vegetation height for each plot to create a height/cover index.

To determine variations in biomass and carbon accumulation between the two sites, herbaceous biomass samples were harvested in 2019, 2020, and 2021. Biomass samples were air or oven-dried at 60° C until the weight of the biomass no longer fluctuated (approximately 48 hours) (described in Chapter 2). Carbon content of herbaceous vegetation was assumed to be 47.5 % based on Zehetgruber et al. (2017).

4.3.2 LiDAR data processing and scaling biomass to the Cameron Valley

Pre-processing of LiDAR range, GNSS position, and trajectory orientation to produce a point cloud was conducted using LMS software (LiDAR Mapping Suite, proprietary software from Teledyne Optech). Following pre-processing, TerraScan (TerraSolid, Finland) was used to classify and remove laser return outliers that did not represent vegetation or the terrain surface. LiDAR returns (points) classified as ground using the shortwave infrared (1550 nm) and near-infrared (1064 nm) wavelengths in 2018 were used as the ground surface for all following years. Vegetation height and cover were lowest during the 2018 LiDAR survey, limiting the interference of vegetation on the ground classification and reducing the inclusion of short vegetation in ground classified points. LiDAR returns were classified as short vegetation, up to 2 m above the ground surface, based on the maximum vegetation height observed in the field. Tall vegetation was classified as > 2 m above the ground surface and represents remaining tree boles and burnt canopy. To maximize point density, the returns from all three channels were included in the analysis.

To model vegetation height in the Cameron Valley bottom, a Digital Elevation Model (DEM) was created using the 2018 LiDAR returns classified as ground. The 2018 DEM was created with a 1 m grid cell using Triangulation with Linear Interpolation in Surfer 12 (Golden Software, United States). Digital Surface Models (DSMs) were created for the 2018, 2019, 2020, and 2021 LiDAR datasets using LiDAR returns classified as short vegetation (0 – 2 m above the

2018 ground surface). The maximum elevation value within a 1 m grid cell was used to create the DSM. Canopy Height Models (CHMs) were created by subtracting the DEM from the DSMs in ArcGIS Pro (ESRI, United States) to provide an estimate of vegetation height above ground. To estimate and remove standing tree boles, CHM grid cells with a value ≥ 2 m were set to null and removed from the analysis. To identify the appropriate resolution for analysis at the valley scale, CHMs representing maximum vegetation height at a 1 m resolution were aggregated to three lower resolutions (2 m, 5 m, 10 m) using the mean of the maximum values. Aggregating height estimates to lower resolutions aids in providing data in regions where point densities are low and cannot accurately represent vegetation structure at a 1 m resolution.

The three wavelengths of the Optech Titan sensor allow for the computation of vegetation indices similar to those used in optical remote sensing. LiDAR returns < 2 m above the ground surface (including ground and short vegetation) were isolated and the intensity values for each wavelength (532 nm, 1064 nm, 1550 nm) were rasterized using the minimum, maximum, and mean intensity values within each grid cell (1 m, 2 m, 5 m, and 10 m). ArcGIS Pro was used to compute the active Normalized Burn Ratio (aNBR) [Equation 3.1]. The aNBR formula uses the high reflectance of NIR energy from healthy vegetation, and the high reflectance of SWIR energy from scorched ground to identify burn severity. The contrast of healthy vegetation and burned ground means that as vegetation regrows, the aNBR values should approach + 1, while burned areas will have negative values, with the most severely burnt regions being close to – 1 (Chasmer et al., 2017; Gerrand et al., 2021).

$$aNBR = \frac{(1064\ nm\ -\ 1550\ nm)}{(1064\ nm\ +\ 1550\ nm)} \qquad \textbf{[Equation 4.1]}$$

The intensity of LiDAR returns diminishes slightly with distance from the center of the scanline. To evaluate the potential impact, data were processed with no overlap between scanlines and full (50 %) overlap between scanlines to determine the method that had the strongest correlation with field validation data. It was determined that the inclusion of all returns from the 50 % overlap region provided the strongest correlation with field measured biomass and vegetation height and was therefore used for further analysis.

4.3.3 Environmental drivers of vegetation regeneration

Within complex montane ecosystems, spatial variability of vegetation growth may be influenced by environmental drivers such as topography and proximity to water. Therefore, this study utilized Forest-based Regression to predict vegetation height for each year following the Kenow Wildland Fire and potential interactions with abiotic environmental drivers (Hudak et al., 2012; McCarley et al., 2020). Forest-based regression creates decision trees and uses the gini statistics to split each node and repeats variations of the model until the most common classification or regression is selected (Hudak et al., 2012).

Vegetation height derived from LiDAR CHMs was used as the variable to predict at three different scales: i) a 6 ha area around the moist site and dry site, representing local variability within and beyond the sites; ii) a 16 ha rectangular region that includes both the moist and dry site for a broader assessment, and finally iii) at the valley bottom scale, a 537 ha region defined by a break in slope between valley bottom and surrounding hill slopes. The valley bottom was used, as opposed to side slopes, as this was the region of the local montane ecosystem where post-fire recovery was observed first, and thus meaningful observations of regeneration could be determined. Within each of these areas (i) through (iii), vegetation height was binned into 10 cm increments from the ground to the tallest vegetation height per year. Random points were distributed proportionally based on the area that each vegetation height bin occupied within the study scale. Each point contained an x, y position coordinate and a z-coordinate representative of the vegetation height within the raster cell where it was located. The Akamina Parkway (main roadway located in Cameron Valley) and a 15 m buffer on each side of the road were excluded from analysis due to anthropogenic disturbance and vegetation management, including cutting down trees and grading the sides of the road in 2020. In total, 885 points were distributed in the valley bottom (ii), 100 points in the combined dry and moist sites (iii), and 50 points for each study site.

Environmental variables evaluated as predictors of vegetation height were derived from LiDAR data and included elevation, slope, aspect, minimum distance to Cameron Creek, topographic position index (TPI), and modelled incoming solar radiation (Solar Analyst, ESRI). The methods used to process each variable are included in Table 3.2. All environmental variables were processed at a 1 m, 5 m, and 10 m cell resolution to identify immediate (1 m) to proximal (> 10 m) influences on vegetation growth. To remove auto-correlating variables that skew Forest-based regression predictions, a correlation matrix was used to determine the coefficient of determination (R^2) between each variable. Environmental variables that correlated with an $R^2 > 0.60$ were investigated to remove the least influential of the two variables. In this analysis, there were no two independent variables that demonstrated an $R^2 > 0.60$, so all variables were included in the Forest-based regression model. The Forest-based regression model was run for each year and each scale (i through iii), with tree sizes of 500, 1500, and 5000 to identify the strongest model. Leaf size and tree depth were automatically determined based on the number of variables included in the prediction. To train and validate the model, 30 % of training data were randomly set aside for independent validation and models were run with both one and 50 validation runs. The influence of each environmental variable was determined by its percent contribution to the prediction. Identifying the influence of environmental variables on vegetation height means that the drivers of spatial and temporal variation in vegetation growth can be identified.

Table 4.2 Methods used to process environmental variable data to be used in the Forest-based regression model.

Variable	Method
Elevation	Derived from a DEM that was created using triangular irregular networks (TIN) from 2018 LiDAR returns classified as ground in TerraScan.
Slope	Calculated based on a 3x3 window to determine the slope of each cell in degrees. Derived from the LiDAR-based 2018 DEM.
Aspect	Calculated based on a 3x3 planar window to determine the aspect of each cell in degrees, where 0° and 360° represent north.
Distance to Cameron Creek	Calculated using the Near tool which calculates the distance from a point (Forest-based regression point) to another feature (Cameron Creek) using a geodesic approach to account for topographic variance.
Topographic position index (TPI)	Calculated based on the extension by Jenness (2006). TPI determines if a cell is above or below the cells in a surrounding search window. Regions with a negative TPI represent valleys, depressions, and canyons. While positive TPI represents hilltops and ridges. TPI calculations were conducted using a circular neighbourhood at sizes ranging from five to 120 cells. TPI grids with different sized neighbourhoods were used in the Forest-based regression to identify the most influential resolution. TPI with a 20 m radius neighbourhood was used in the regression model.
Incoming solar radiation	Incoming solar radiation was calculated based on the amount of incoming solar radiation for each cell based on the latitude, sky size, time of year, cloud cover, and transmissivity. The time used was from May 1st to September 30th of each year to capture the growing season.

4.3.4 Statistical methods and models

To determine the significance of vegetation growth from year to year, a t-test with a 95 % confidence interval was used in SPSS (IBM, United States) for parametric data, while the Wilcoxon signed-rank test was used for non-parametric data as determined by one-sample Shapiro-Wilk and Kolmogorov-Smirnov. The difference between datasets was considered significant when $p < 0.05$ using a two-tailed significance test. To identify the quality of the relationship between LiDAR and field validation data, the adjusted R^2 and significance from linear regression in SPSS were used. In the case of scaling biomass quantities to the valley bottom based on field measurement and LiDAR derived aNBR, the linear regression equation was used to provide an estimate of biomass.

4.4 RESULTS

4.4.1 LiDAR-based height models

LiDAR-modelled vegetation height at a 1 m, 2 m, 5 m, and 10 m resolution were compared with field measured vegetation metrics (Table 3.3). The optimal resolution for modelling vegetation height was the LiDAR 1 m maximum ($R2 = 0.33$, $p < 0.001$) or 10 m mean of the maximum vegetation heights ($R2 = 0.33$, $p < 0.001$). However, the 1 m maximum height had the strongest correlation with all vegetation metrics measured in the field, including the only significant correlation with field measured biomass (Table 3.3). LiDAR underestimated vegetation height in all years of the study, with the greatest difference existing between modelled vegetation at the plot level and field measured vegetation in 2019 (Table 3.4). Modelled vegetation at the valley scale did not correspond with decreasing mean vegetation height observed between 2019 and 2020 but did have a corresponding decrease in vegetation height from 2020 to 2021 (Table 3.4).

Table 4.3 Linear regression results between LiDAR derived maximum vegetation height (1 m), mean of the maximum vegetation height (2 m – 10 m), and plot-level field measurements for the moist and dry sites in 2020 and 2021. R^2 is displayed for each relationship with the p-value in brackets.

LiDAR-derived CHM mean compared to field vegetation metrics				
Field Variable	1 m maximum height	2 m mean of the maximum height	5 m mean of the maximum height	10 m mean of the maximum height
Height (n = 91)	0.33 (<0.001)	0.20 (<0.001)	0.16 (<0.001)	0.33 (<0.001)
Cover (n = 60)	0.42 (0.001)	0.36 (<0.001)	0.23 (<0.001)	0.32 (<0.001)
Gcc (n = 91)	0.44 (<0.001)	0.22 (<0.001)	0.17 (<0.001)	0.38 (<0.001)
gcc * height index (n = 91)	0.38 (<0.001)	0.22 (<0.001)	0.18 (<0.001)	0.37 (<0.001)
Biomass dry weight (n = 19)	0.45 (0.002)	0.21 (0.064)	0.08 (0.242)	0.11 (0.16)

Table 4.4 Comparison of LiDAR-modelled average vegetation height at the valley scale and plot scale with field-measured vegetation heights. 2018 data were excluded from analysis due to too few vegetation plot measurements. The mean vegetation height sample n-values and standard deviation are included for 2019 to 2021.

		Modelled valley vegetation (m)	Field-measured vegetation (m)	Modelled plot vegetation (m)
2019	Mean	0.41	0.58	0.29
	Standard deviation	0.38	0.20	0.12
	n	5.04×10^6	31	31
2020	Mean	0.48	0.54	0.40
	Standard deviation	0.37	0.24	0.18
	n	5.26×10^6	58	58
2021	Mean	0.46	0.50	0.41
	Standard deviation	0.42	0.22	0.27
	n	5.12×10^6	32	32

4.4.2 LiDAR-based biomass models

LiDAR-derived aNBR had significant correlations with field measured vegetation metrics across all resolutions used. LiDAR mean aNBR correlation with vegetation metrics including height, cover, and gcc was strongest at a 2 m resolution (Table 3.5). However, LiDAR mean aNBR at a 1 m resolution had the strongest correlation with biomass ($R^2 = 0.77$, $p < 0.001$) and the correlation decreased in lower resolutions (Table 3.5). The linear regression equation ($y = 686.9 * \text{aNBR} + 574.4$) was developed based on the relationship between field-measured biomass and mean aNBR at a 1 m resolution and was used to estimate biomass within the study sites and the valley bottom. At the plot level, the LiDAR aNBR biomass model overestimated field-measured biomass by up to 119 g m^{-2} and underestimated biomass by up to 168 g m^{-2}. The sum of the difference between measured and modelled biomass was -0.66 g m^{-2}, indicating that LiDAR aNBR modelled biomass was representative of field-measured biomass.

Table 4.5 Linear regression results between LiDAR derived mean aNBR values and plot-level field measurements for the moist and dry sites in 2020 and 2021. R^2 is displayed for each relationship with the p-value in brackets.

LiDAR-derived aNBR compared to vegetation metrics				
Field Variables	1 m mean aNBR	2 m mean aNBR	5 m mean aNBR	10 m mean aNBR
Height (n = 87)	0.32 (<0.001)	0.34 (<0.001)	0.14 (<0.001)	0.08 (0.01)
Cover (n = 56)	0.38 (<0.001)	0.46 (<0.001)	0.15 (0.003)	0.12 (0.009)
gcc (n = 87)	0.40 (<0.001)	0.50 (<0.001)	0.24 (<0.001)	0.14 (0.001)
gcc * Height index (n = 87)	0.36 (<0.001)	0.40 (<0.001)	0.19 (<0.001)	0.11 (0.002)
Biomass dry weight (n = 19)	0.77 (<0.001)	0.53 (<0.001)	0.30 (<0.001)	0.29 (0.003)

At the valley scale, mean LiDAR-modelled biomass increased from 2018 (122 g m^{-2}) to 2019 (322 g m^{-2}) before decreasing in 2020 (231 g m^{-2}) (Table 3.6; Figure 3.2). This follows the same pattern of biomass decrease observed in field measurements from 2019 to 2020 (Table 3.6). In contrast, LiDAR-modelled mean biomass at both the valley and plot scale was found to increase from 2020 to 2021, while field measured biomass decreased over this period.

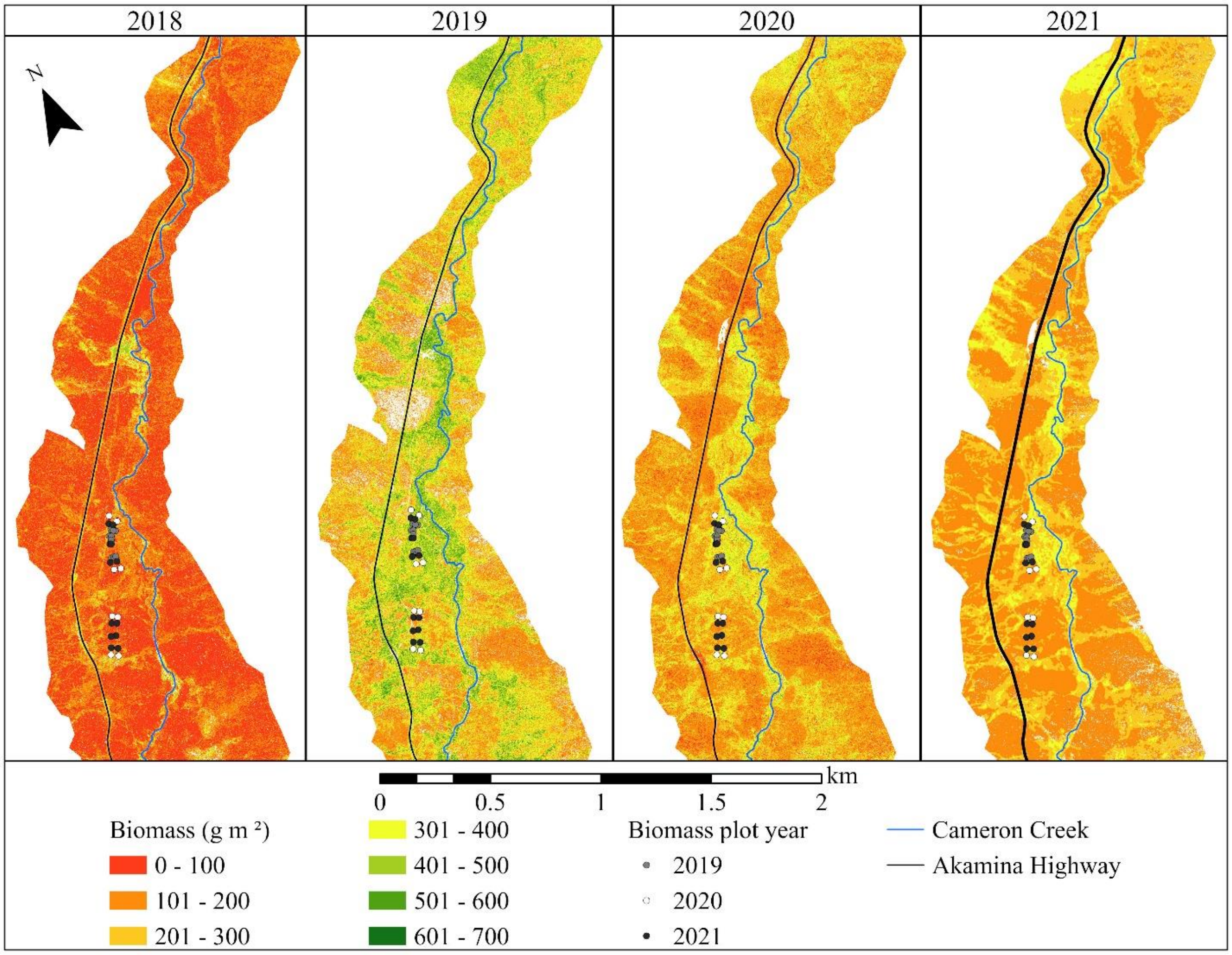

Figure 4.2 LiDAR modelled biomass based on a linear regression equation applied to LiDAR derived aNBR. Map frames represent 2018 (left), 2019 (center-left), and 2020 (center-right), and 2021 (right) biomass quantities (g m^{-2}).

Table 4.6 Comparison of LiDAR modelled biomass at the valley and plot scale with field measured biomass from 2019 to 2021. 2018 biomass at the plot level was excluded due to there being no biomass harvest that year. The n-values and standard deviation are included below the average biomass.

		Modelled valley biomass (g m^{-2})	Field-measured biomass (g m^{-2})	Modelled plot biomass (g m^{-2})
2018	Mean	122	NA	NA
	Standard deviation	70.2		
	n	4.23×10^6		
2019	Mean	322	368	378
	Standard deviation	113.3	69.2	67.3
	n	4.93×10^6	9	9
2020	Mean	231	235	201
	n	5.11×10^6	7	7
	Standard deviation	85.1	69.5	72.6
2021	Mean	235	208	219
	Standard deviation	60.6	165.7	18.8
	n	5.12×10^6	12	12

4.4.3 Local abiotic site conditions impacting spatial variability of vegetation change

The Forest-based regression models used to predict vegetation height had varying results based on the scale and year of the data used. Generally, when considering all scales, the model best predicted vegetation in 2020, and had the highest predicted R^2 in the moist site ($R^2 = 0.74$, $p < 0.001$). The Forest-based regression predicted R^2 was greatest in the moist site ranging from 0.17 ($p = 0.03$) in 2018 to 0.74 ($p < 0.001$) in 2020 and was lowest at the valley scale with predicted R^2 values between 0.04 ($p = 0.006$) in 2018 and 0.10 ($p < 0.001$) in 2020 (Table 3.7).

Table 4.7 Forest-based regression training and predicted accuracy. R^2 is displayed for each relationship with the significance in brackets. The most influential variables ranked (one, two, and three) based on the prediction model.

	Model Performance		**Variable importance**		
	Training R^2	**Predicted R^2**	**Variable one**	**Variable two**	**Variable three**
Full study area					
2018	0.89 (<0.001)	0.02 (0.06)	Distance to creek (23 %)	Elevation (21 %)	TPI (19 %)
2019	0.91 (<0.001)	0.02 (0.43)	Aspect (27 %)	Elevation (19 %)	Slope (18 %)
2020	0.89 (<0.001)	**0.34 (0.001)**	TPI + solar radiation (26 %)	Distance to creek (24 %)	Elevation (22 %)
2021	0.88 (<0.001)	0.17 (0.03)	TPI (29 %)	Aspect (25 %)	Distance to creek (23 %)
Moist study site					
2018	0.83 (<0.001)	0.17 (0.30)	TPI (25 %)	Slope (21 %)	Distance to creek + Aspect (19 %)
2019	0.91 (<0.001)	0.37 (0.05)	Slope (26 %)	Solar radiation (19 %)	TPI (16 %)
2020	0.91 (<0.001)	**0.74 (<0.001)**	Aspect (30 %)	Solar radiation (25 %)	Distance to creek (23 %)
2021	0.86 (<0.001)	0.31 (0.07)	TPI (23 %)	Slope (22 %)	Distance to creek (18 %)
Dry study site					
2019	0.89 (<0.001)	**0.73 (<0.001)**	Elevation (25 %)	TPI (23 %)	Solar radiation (18 %)
2019	0.83 (<0.001)	0.24 (0.12)	Aspect (26 %)	Slope (25 %)	Elevation (18 %)
2020	0.83 (<0.001)	0.30 (0.06)	Distance to creek (31 %)	TPI (27 %)	Aspect (22 %)

2021	0.74 (<0.001)	0.27 (0.08)	TPI (28 %)	Solar radiation (26 %)	Slope (25 %)
Valley bottom					
2018	0.90 (<0.001)	0.04 (0.006)	Slope (23 %)	Distance to creek (21 %)	Solar radiation + elevation (19 %)
2019	0.92 (<0.00)	0.06 (0.001)	TPI + Distance to creek (21 %)	Solar radiation + slope (20 %)	Elevation (19 %)
2020	0.92 (<0.001)	**0.10 (<0.001)**	Solar radiation (21 %)	Elevation + TPI + Distance to creek (20 %)	Slope (19 %)
2021	0.91 (<0.001)	0.04 (0.004)	Elevation (21 %)	Solar radiation + Distance to creek (20 %)	TPI + Slope (19 %)

The abiotic factors with the greatest influence on vegetation height, determined from LiDAR-based spatial derivatives were local TPI, distance to Cameron Creek, and slope. TPI and distance to Cameron Creek can be used as proxies for moisture availability, indicating that moisture drives spatial variability in growth rates in the early years post-fire. The influence of factors such as TPI and distance to Cameron Creek on vegetation growth can be identified within the valley bottom (Figure 3.2). Modelled biomass accumulation in 2018 is concentrated around Cameron Creek and in rills leading to the creek. In 2019, biomass accumulation expanded from these established regions of growth. This approach describes a portion of the variability in regeneration as other drivers such as soil nutrient availability, soil depth, and soil type cannot be spatially determined using LiDAR.

Analysis of the spatial distribution of vegetation height confirms observations of variable importance in the Forest-based regression model. In 2020, regions with low-lying topographic positions had an average vegetation height of 0.59 m, while regions with a raised topographic position had an average of 0.45 m. When examining the change in vegetation height with distance from Cameron Creek it was found that the tallest vegetation in 2020 and 2021 was within 50 m of the creek and decreased with distance. Both 2020 and 2021 were warm dry years, indicating that moisture availability with proximity to Cameron Creek is important in years of drought. Although not of high influence in the Forest-based regression model, vegetation height was found to increase with elevation in the Cameron Valley. Despite height variation being small, the relation between vegetation height and elevation was moderate but significant ($R^2 = 0.47$, $p = 0.04$).

4.5 DISCUSSION

4.5.1 LiDAR observation of vegetation regeneration

LiDAR-modelled vegetation height provided weak to moderate correlations with field measured biomass. Results from this study indicate that LiDAR-derived CHMs had moderate correlations with biomass ($R^2 = 0.45$, $p < 0.002$) (Table 3.4), underperforming the LiDAR-derived CHMs ($R^2 = 0.80$) used to model tree biomass by Hudak et al (2012). However, studies such as that by Hudak et al. (2012), focused on aboveground tree biomass, while this study focused on post-fire vegetation regeneration composed primarily of short herbaceous vegetation. It is expected that deadfall within regenerating vegetation and remaining short tree boles within the post-fire environment are sources of noise that reduce the ability to effectively model vegetation height. As forest succession continues and the species composition shifts to shrub or short conifer forests, it is expected that the effectiveness of LiDAR CHMs for capturing the variability in vegetation height will increase as the range between vegetation and the ground increases.

The relationship between LiDAR derived height and field heights identified using linear regression were strongest at the 1 m resolution ($R^2 = 0.33$, t-test; $p < 0.001$; Table 3.3). As with the spectral data, LiDAR derived height had weak correlations with vegetation height in the moist site. However, correlations were strengthened through the inclusion of the dry site due to the increased sample size and variance in vegetation height measurements. Using multispectral LiDAR data, comparisons between LiDAR-derived maximum vegetation height and field metrics including vegetation height, cover, gcc, and biomass were strongest at 1 m cell resolutions (Table 3.4). At the time of the study, vegetation height and cover were relatively homogenous over large portions of the study sites, particularly the moist site (Chapter 2, Figure 2.8). As vegetation continues to regenerate and the ecosystem transitions from an early herbaceous to a shrubby or conifer-dominated ecosystem, it is expected that lower cell resolutions will become less effective as variation in vegetation cover increases. The efficacy of the 1 m resolution in this early post-fire environment may provide consistency as finer cell resolution within the LiDAR may become more effective.

4.5.2 LiDAR biomass models

Modelled biomass accumulation in the Cameron Valley bottom increased significantly from 2018 to 2019 (Wilcoxon; $p < 0.001$; Table 3.6), as expected with time since fire. However, reductions in biomass from 2019 to 2020 were not anticipated. The decrease in modelled biomass is associated with observed decreases in field measurements and is likely related to abnormally warm, dry annual weather conditions (Chapter 2, Figure 2.7). However, potential influences on LiDAR properties were investigated to eliminate sensor error as an influence on decreasing modelled biomass.

Variation in ground surface moisture can alter reflected LiDAR returns in the NIR and SWIR by absorbing more energy and decreasing the return intensity, leading to an underestimation of vegetation when using a spectral index such as aNBR (Lobell & Asner, 2002). In the week prior to the 2019 LiDAR survey there was ~ 21 mm of precipitation, while the week prior to the 2020 LiDAR there was 0 mm of precipitation. VWC also varied within the moist site from 29 % in 2019 to 20 % in 2020. Despite higher precipitation and VWC in 2019, return intensities in the NIR were greater than in 2020, indicating that moisture did not influence the decrease in aNBR-modelled biomass predictions.

An alternative influence on the LiDAR spectral properties is the structure, cover, and species of the vegetation. Taller vegetation within the valley bottom may increase the number of split laser pulses, reducing the peak amplitude of return intensity (Garroway et al., 2011). However, vegetation height and gcc did not vary significantly from 2019 to 2020 (Chapter 2, Figure 2.8), indicating that vegetation structure did not increase the number of split laser pulses. LiDAR spectral properties are also influenced by atmospheric conditions. Variations in atmospheric turbidity, caused by wind and smoke common in montane regions during the summer months, can cause variations in spectral properties between annual data collections. In the future, return intensities should be normalized using an invariant calibration site to reduce the influence of atmospheric conditions.

Finally, the reduction in biomass from 2019 to 2020 may be an accurate reflection of a change in the Cameron Valley (Figure 3.2). Despite annual precipitation in 2020 being 52 mm greater than in 2019, the growing season received 106 mm less precipitation which could inhibit vegetation growth and result in early senescence. Decreases in biomass observed in field measurements could be the result of variations in the spatial distribution of harvested samples. However, the same decreases were observed in the LiDAR-modeled biomass at the plot and valley scale, indicating that 2020 may have been a year of reduced vegetation growth (Table 3.6). Continued hot, dry conditions in 2021 may explain the reduced biomass measured in the field from 2020 to 2021, particularly in the dry site. Although LiDAR-modelled biomass increased at both the plot and valley scale, increases were small and fell within the standard deviation of field measured biomass.

4.5.3 Importance of local abiotic site conditions

Of the abiotic site conditions considered within the moist and dry sites, it was found that moisture proxies including TPI and distance to Cameron Creek had the greatest influence on vegetation distribution and height (Table 3.7). Vegetation height was greatest in areas with a low TPI, indicating that vegetation accumulates in depressions and low-lying areas that accumulate moisture and are closest to the water table. These results are consistent with studies that have identified moisture availability as a driver of regeneration in montane environments (Harvey et al., 2016; Ireland & Petropoulos, 2015; Swetnam et al., 2017).

In the valley bottom, where moisture is assumed to be relatively abundant, the influence of topography and incoming solar radiation on the distribution and height of vegetation becomes important. It was determined that in the Cameron Valley, vegetation height was greater with increasing elevation. Elevation is often used as a measure of moisture availability and temperature control (Dodson & Root, 2013; Rother & Veblen, 2016; Turner et al., 2004), and more locally, is an indicator of soil characteristics. In the Cameron Valley, the cumulative annual precipitation ranged from approximately 751 mm in lower elevations (~ 1500 m) to approximately 1195 mm at higher elevations (~ 1700 m). Temperature was also found to decrease by approximately 1.6° C over the same elevation range. Analysis of climate data across elevation gradients in Waterton confirms what is stated in the literature, that elevation in Waterton can be used as a proxy for changes in temperature and precipitation.

With regards to local environmental drivers of vegetation height, Forest-based regression predictions of vegetation height resulted in a low coefficient of determination (R^2) in both the study sites and across the valley bottom (Table 3.7). The efficacy of this model may increase with the inclusion of additional variables such as soil characteristics, or as vegetation grows, species composition changes, and variation in vegetation height increases.

4.6 CONCLUSION

Overall, multispectral LiDAR-derived aNBR-based biomass models were demonstrated to be a useful tool for modelling the distribution of biomass within the Cameron Valley bottom. Although no field biomass data is available for 2018, the modelled increase in biomass was anticipated from 2018 to 2019 but declines in biomass in 2020 and 2021 were not expected. LiDAR models indicate that biomass accumulation is greatest in regions surrounding Cameron Creek and in rills along the toe of the valley. While LiDAR underestimated measured vegetation height in the moist site, correspondence improved with years since fire, and in areas without tall grasses, which do not contribute enough surface area to produce a laser pulse return from the top of the plant. Forest-based regression models consistently indicate that proxies for moisture such as TPI and the shortest distance to Cameron Creek are the most influential environmental drivers of biomass accumulation. However, during hot dry years such as 2020, energy receipt had the strongest influence on the spatial variability of biomass in the moist site. The results of this study show how biomass accumulates over space and time since fire using airborne LiDAR. Continued assessment will be beneficial for classifying and quantifying seedling biomass and timing of the transition from a herbaceous-dominated to a conifer-dominated landscape.

CHAPTER 4: CONCLUSION

5.1 SUMMARY OF RESEARCH

This thesis aimed to quantify vegetation change in moisture endmember sites and determine the efficacy of LiDAR and RPAS for identifying changes in post-fire vegetation structure and distribution over the first four years following a severe montane wildland fire. The results of this study contribute to the understanding of how severely burned montane forests regenerate under warmer, drier conditions that differ from the climate of 150 - 200 years ago. These results provide a baseline understanding of forest resilience under current climate conditions.

Chapter two compared rates of post-fire vegetation growth between two moisture endmember sites and RPAS SfM-modelled vegetation characteristics. When compared with the dry montane valley site, increased VWC in the moist site enhanced herbaceous vegetation regeneration, resulting in greater rates of vegetation height, lateral expansion of leaf cover, greater biomass, and greater species richness. However, the greatest conifer seedling establishment was found in the dry study site. This may indicate that high-density herbaceous vegetation may lead to increased competition for resources and a reduction in conifer seedlings. Alternatively, pre-fire tree distribution and factors, such as soil composition and nutrients may have a greater influence on lodgepole pine seedling density.

To quantify the spatial variability of vegetation height and cover over time RPAS optical images were also used. Here, it was determined that the RPAS gcc index and SfM point clouds could be used to estimate vegetation height and biomass. RPAS SfM modelled vegetation correlated well with field measured vegetation height ($R^2 = 0.54$, $p < 0.001$) but was ineffective at modelling biomass ($R^2 = 0.0007$, $p = 0.129$) measured over time. However, RPAS gcc had significant correlations with both plot gcc ($R^2 = 0.44$, $p = 0.129$) and biomass ($R^2 = 0.55$, $p = 0.002$). These results indicate that RPAS optical and SfM data can be used to effectively estimate the structure and distribution of short, early-stage vegetation regeneration, making it a viable tool for monitoring early post-fire vegetation regeneration.

Chapter three of this study focused on using LiDAR to develop a valley-scale model of biomass and identifying the environmental drivers that influence the spatial distribution of vegetation. Multispectral LiDAR aNBR indices were significantly correlated ($R^2 = 0.77$, $p < 0.001$) with field-measured biomass. The efficacy of LiDAR aNBR for estimating biomass exceeds that of the RPAS models in Chapter 2 ($R^2 = 0.74$, $p = 0.129$). This indicates that the use of raster-based indices based on energy partitioning from plants and bare surface (such as aNBR or gcc) are more reliable for the identification of biomass growth and expansion than structural-based or point cloud methods. This is likely due to ground level noise from deadfall that exists within regenerating vegetation structure which is difficult to separate and exclude.

The correlation between LiDAR derived aNBR and field measured biomass facilitates modelling of biomass accumulation at the valley scale. Modelled biomass visually indicates that accumulation is greatest in regions proximal to Cameron Creek and depressions or rills from the mountain slopes. This was confirmed through Forest-based Regression, which identified the most influential abiotic variables on biomass accumulation to be TPI, distance to Cameron Creek, slope, and incoming solar radiation. The identified abiotic variables can be used as proxies for moisture availability, indicating that moisture is a critical driver of post-fire vegetation regeneration.

This study demonstrates the importance of moisture availability on post-fire regeneration, both at the site level and with interannual climate variability, following the Kenow Wildland Fire. In the first four years post-fire, vegetation regeneration has been greatest in moist regions of the

Cameron Valley, and in years with cooler growing season temperatures and higher growing season precipitation. Remote sensing methods using LiDAR and RPAS effectively modelled initial vegetation regeneration within this complex montane environment. These methods may be important tools for land managers to continue monitoring post-fire regeneration and model future post-fire regeneration.

5.2 FUTURE CONSIDERATIONS

Despite the consistent time series data over the first four years post-fire, this study has limitations. First, this study combined field and remote sensing methods, as a result, plots established for field purposes were also used as validation of LiDAR data. The scale established for field plots was not ideal for the remote sensing component of the study. Low point density within vegetation plots limits direct model transfer to a sample-based approach with some plots only represented by one or two lidar points. This issue could be addressed by establishing larger field plots, potentially a 5 m radius, to increase LiDAR point density and create a more robust comparison. However, larger field plots would be more time-consuming to measure and would also increase bias due to trampling of short herbaceous vegetation during measurement, as these sites were frequently measured each year.

Second, the ability to compare LiDAR and RPAS datasets was limited by distortion within the RPAS SfM point clouds. Distortion along the edge of the point cloud occurs when there is not enough image overlap, this is a common problem with SfM. Due to the distortion, RPAS and LiDAR point clouds could not be accurately aligned across the entire plot extent. Expanding the study area of the RPAS survey would reduce the edge effect, making the two datasets more comparable. This adaptation may be difficult due to the limited battery life of the system used and longer flight times, combined with the operational constraints of collecting data in a National Park.

RPAS surveys could be conducted with an increased flight height, this would increase the area surveyed but would decrease the data resolution and further reduce SfM point coordinate accuracy.

This study addresses the current state of regeneration within the Cameron Valley bottom. Future work in this region should continue to expand spatially and temporally. Re-visiting established sites, even at a reduced frequency, will expand our understanding of change and projections for future vegetation growth. As time continues, the focus should shift from the distribution of herbaceous vegetation to shrubby and conifer ‘woody’ vegetation. Understanding the distribution of woody vegetation and the abiotic variables that drive growth will foster an understanding of how this ecosystem will progress in the coming decades. This study demonstrated the potential of LiDAR aNBR data for the estimation of biomass under early post-fire regeneration conditions. Expanding on this relationship could provide a methodology for assessing burn severity within the initial years post-fire.

REFERENCES

Agriculture and Irrigation, Alberta Climate Information Service (ACIS) (2021, May 1). *Current and Historical Alberta Weather Station Data Viewer*. Alberta Climate Information Service. https://acis.alberta.ca

Alberta Environment and Parks (2018, July 1). *Protocols for the measurement of snow water equivalent with a snow pillow*. Alberta Government. https://open.alberta.ca/dataset/c2e1bc58-743b-4910-b46f-c2b1230b8e3b/resource/6eee84be-65ad-4526-93f1-ba1f47a5c353/download/aep-protocols-for-measurement-of-snow-water-equivalent-with-snow-pillow.pdf

Alexiou, S., Deligiannakis, G., Pallikarakis, A., Papanikolaou, I., Psomiadis, E., & Reicherter, K. (2021). Comparing high accuracy t-LiDAR and uav-sfm derived point clouds for geomorphological change detection. *ISPRS international journal of geo-information, 10*(367), 367. doi:10.3390/ijgi10060367

Amiro, B. D., Todd, J. B., Wotton, B. M., Logan, K. A., Flannigan, M. D., Stocks, B. J., . . . Hirsch, K. G. (2001). Direct carbon emissions from canadian forest fires, 1959-1999. *Canadian Journal of Forest Research, 31*(3), 512-525. doi:10.1139/x00-197

Amiro, B., Barr, A., Black, T., Iwashita, H., Kljun, N., McCaughey, J., . . . Orchansky, A. (2006). Carbon, energy and water fluxes at mature and disturbed forest sites, saskatchewan, canada. Agricultural and forest meteorology, 136(3-4), 237-251.

Andrus, R. A., Harvey, B. J., Rodman, K. C., Hart, S. J., & Veblen, T. T. (2018). Moisture availability limits subalpine tree establishment. *Ecology, 99*(3), 567-575. doi:10.1002/ecy.2134

Badgley, G., Field, C. B., & Berry, J. A. (2017). Canopy near-infrared reflectance and terrestrial photosynthesis. Science advances, 3(3), e1602244

Bartowitz, K. J., Higuera, P. E., Shuman, B. N., McLauchlan, K. K., & Hudiburg, T. W. (2019). Post-fire carbon dynamics in subalpine forests of the rocky mountains. *Fire, 2*(4), 58.

Beland, M., Parker, G., Sparrow, B., Harding, D., Chasmer, L., Phinn, S., . . . Strahler, A. (2019). On promoting the use of LiDAR systems in forest ecosystem research. *Forest Ecology and Management, 450*, 117484. doi:10.1016/j.foreco.2019.117484

Besnard, S., Carvalhais, N., Arain, M. A., Black, A., De Bruin, S., Buchmann, N., . . . Desai, A. R. (2018). Quantifying the effect of forest age in annual net forest carbon balance. *Environmental Research Letters, 13*(12), 124018.

Bonnet, V. H., Schoettle, A. W., & Shepperd, W. D. (2005). Postfire environmental conditions influence the spatial pattern of regeneration for pinus ponderosa. *Canadian Journal of Forest Research, 35*(1), 37-47.

Busby, S. U., Moffett, K. B., & Holz, A. (2020). High-severity and short-interval wildfires limit forest recovery in the central cascade range. *Ecosphere, 11*(9), e03247.

Caratti (2006): Point intercept sampling method. USDA Forest Service Gen. Tech. Rep. RMRS-GTR-164-CD. www.fs.fed.us/rm/pubs/rmrs_gtr164

Carter, M. R., & Gregorich, E. G. (2008). *Soil sampling and methods of analysis* (2nd ed.). Boca Raton, Fla: CRC Press.

Carvajal-Ramírez, F., Marques da Silva, J. R., Agüera-Vega, F., Martínez-Carricondo, P., Serrano, J., & Moral, F. J. (2019). Evaluation of fire severity indices based on pre- and post-fire multispectral imagery sensed from uav. *Remote sensing (Basel, Switzerland), 11*(9), 993. doi:10.3390/rs11090993

Chasmer, L., Hopkinson, ., Veness, T., Quinton, W., Baltzer, J., (2014). A decision-tree classification for low-lying complex land cover types within the zone of discontinuous permafrost. *Remote Sensing of Environment, 143, 73-84.* https://doi.org/10.1016/j.rse.2013.12.016.

Chasmer, L., Hopkinson, C., Petrone, R., & Sitar, M. (2017). Using multitemporal and multispectral airborne LiDAR to assess depth of peat loss and correspondence with a new active normalized burn ratio for wildfires: Depth of burn of peat soils using LiDAR. *Geophysical research letters, 44*(23), 11-11,859. doi:10.1002/2017GL07548

Chen, S., McDermid, G., Castilla, G., & Linke, J. (2017). Measuring vegetation height in linear disturbances in the boreal forest with uav photogrammetry. *Remote sensing (Basel, Switzerland), 9*(12), 1257. doi:10.3390/rs9121257

Coop, J. D., Massatti, R. T., & Schoettle, A. W. (2010). Subalpine vegetation pattern three decades after stand-replacing fire: Effects of landscape context and topography on plant community composition, tree regeneration, and diversity. *Journal of vegetation science, 21*(3), 472-487.

Current and Historical Alberta Weather Station Data Viewer. (2022). Retrieved 6 January 2022, from https://acis.alberta.ca/weather-data-viewer.jsp

Dandois, J. P., & Ellis, E. C. (2010). Remote sensing of vegetation structure using computer vision. *Remote Sensing, 2*(4), 1157-1176.

Dodson, E. K., & Root, H. T. (2013). Conifer regeneration following stand-replacing wildfire varies along an elevation gradient in a ponderosa pine forest, oregon, USA. *Forest Ecology and Management, 302*, 163-170.

Donato, D. C., Fontaine, J. B., Campbell, J. L., Robinson, W. D., Kauffman, J. B., & Law, B. E. (2009). Conifer regeneration in stand-replacement portions of a large mixed-severity wildfire in the klamath–siskiyou mountains. *Canadian Journal of Forest Research, 39*(4), 823-838.

Donato, D. C., Harvey, B. J., & Turner, M. G. (2016). Regeneration of montane forests 24 years after the 1988 yellowstone fires: A fire-catalyzed shift in lower treelines? *Ecosphere, 7*(8), e01410.

Dong, P., & Chen, Q. (2018). *LiDAR remote sensing and applications* (1 ed. Vol. 1). Boca Raton, FL: CRC Press, Taylor & Francis Group

Environment Canada. (2022). *Historical Data.* Government of Canada. Hourly Data Report for July 19, 2023 - Climate - Environment and Climate Change Canada (weather.gc.ca)

Fellows, A. W., Flerchinger, G. N., Lohse, K. A., & Seyfried, M. S. (2018). Rapid recovery of gross production and respiration in a mesic mountain big sagebrush ecosystem following prescribed fire. Ecosystems, 21(7), 1283-1294.

Garcia, M., Saatchi, S., Casas, A., Koltunov, A., Ustin, S., Ramirez, C., . . . Balzter, H. (2017). Quantifying biomass consumption and carbon release from the california rim fire by integrating airborne LiDAR and landsat oli data. *Journal of geophysical research. Biogeosciences, 122*(2), 340-353. doi:10.1002/2015JG003315

Garroway, K., Hopkinson, C., & Jamieson, R. (2011). Surface moisture and vegetation influences on LiDAR intensity data in an agricultural watershed. *Canadian Journal of Remote Sensing, 37*(3), 275-284. doi:10.5589/m11-036

Gendreau-Berthiaume, B., Macdonald, S. E., & Stadt, J. J. (2018). Importance of the canopy in determining on-going regeneration and stand successional development in lodgepole pine forests. *Journal of vegetation science, 29*(2), 213-225.

Goulden, M. L., McMillan, A., Winston, G., Rocha, A., Manies, K., Harden, J. W., & Bond-Lamberty, B. (2011). Patterns of NPP, GPP, respiration, and NEP during boreal forest succession. Global Change Biology, 17(2), 855-871.

Gerrand, S., Aspinall, J., Jensen, T., Hopkinson, C., Collingwood, A., & Chasmer, L. (2021). Partitioning carbon losses from fire combustion in a montane valley, alberta canada. *Forest Ecology and Management, 496*, 119435. doi:10.1016/j.foreco.2021.119435

Goodbody, T., Coops, N. C., Hermosilla, T., Tompalski, P., & Crawford, P. (2018). Assessing the status of forest regeneration using digital aerial photogrammetry and unmanned aerial systems. *International journal of remote sensing, 39*(15-16), 5246-5264. doi:10.1080/01431161.2017.1402387

Goodbody, T., Coops, N. C., Marshall, P. L., Tompalski, P., & Crawford, P. (2017). Unmanned aerial systems for precision forest inventory purposes: A review and case study. *The Forestry Chronicle, 93*(1), 71-81.

Government of Canada. (2020). Parks Canada attendance 2019-20. Retrieved from https://open.canada.ca/data/en/dataset/96d26ef3-bf21-4ea5-a9c9-80b909fbcbc2

Hanes, C. C., Wang, X., Jain, P., Parisien, M.-A., Little, J. M., & Flannigan, M. D. (2019). Fire-regime changes in canada over the last half century. *Canadian Journal of Forest Research, 49*(3), 256-269. doi:10.1139/cjfr-2018-0293

Hansen, W. D., & Turner, M. G. (2019). Origins of abrupt change? Postfire subalpine conifer regeneration declines nonlinearly with warming and drying. *Ecological Monographs, 89*(1), e01340-n/a. doi:10.1002/ecm.1340

Harvey, B. J., Donato, D. C., & Turner, M. G. (2016). High and dry: Post-fire tree seedling establishment in subalpine forests decreases with post-fire drought and large stand-replacing burn patches. *Global Ecology and Biogeography, 25*(6), 655-669. doi:10.1111/geb.12443

Hopkinson, C., Chasmer, L., Gynan, C., Mahoney, C., & Sitar, M. (2016). Multisensor and multispectral LiDAR characterization and classification of a forest environment. *Canadian Journal of Remote Sensing, 42*(5), 501-520.

Hopkinson, C., Chasmer, L., Lim, K., Treitz, P., & Creed, I. (2006). Towards a universal LiDAR canopy height indicator. *Canadian Journal of Remote Sensing, 32*(2), 139-152.

Hopkinson, C., Chasmer, L. E., Sass, G., Creed, I. F., Sitar, M., Kalbfleisch, W., & Treitz, P. (2005). Vegetation class dependent errors in LiDAR ground elevation and canopy height estimates in a boreal wetland environment. *Canadian Journal of Remote Sensing, 31*(2), 191-206.

Hudak, A. T., Strand, E. K., Vierling, L. A., Byrne, J. C., Eitel, J. U., Martinuzzi, S., & Falkowski, M. J. (2012). Quantifying aboveground forest carbon pools and fluxes from repeat LiDAR surveys. *Remote Sensing of Environment, 123*, 25-40.

Ireland, G., & Petropoulos, G. P. (2015). Exploring the relationships between post-fire vegetation regeneration dynamics, topography and burn severity: A case study from the montane cordillera ecozones of western canada. *Applied Geography, 56*, 232-248. doi:10.1016/j.apgeog.2014.11.016

Jenness, J. (2006). Topographic Position Index (TPI). http://www.jennessent.com/arcview/tpi.htm

Jiang, R., Gan, T. Y., Xie, J., Wang, N., & Kuo, C.-C. (2017). Historical and potential changes of precipitation and temperature of alberta subjected to climate change impact: 1900–2100. *Theoretical and applied climatology, 127*(3), 725-739. doi:10.1007/s00704-015-1664-y

Jolly, W. M., Cochrane, M. A., Freeborn, P. H., Holden, Z. A., Brown, T. J., Williamson, G. J., & Bowman, D. M. J. S. (2015). Climate-induced variations in global wildfire danger from 1979 to 2013. *Nature communications, 6*(1), 7537-7537. doi:10.1038/ncomms8537

Kashian, D. M., Romme, W. H., Tinker, D. B., Turner, M. G., & Ryan, M. G. (2006). Carbon storage on landscapes with stand-replacing fires. *Bioscience, 56*(7), 598-606.

Keeley, J. E. (2009). Fire intensity, fire severity and burn severity: A brief review and suggested usage. International Journal of Wildland Fire, 18(1), 116-126.

Kirchmeier-Young, M. C., Zwiers, F. W., Gillett, N. P., & Cannon, A. J. (2017). Attributing extreme fire risk in western canada to human emissions. *Climatic Change, 144*(2), 365-379. doi:10.1007/s10584-017-2030-0

Landhäusser, S. M., Deshaies, D., & Lieffers, V. J. (2010). Disturbance facilitates rapid range expansion of aspen into higher elevations of the rocky mountains under a warming climate. *Journal of Biogeography, 37*(1), 68-76.

Larrinaga, A. R., & Brotons, L. (2019). Greenness indices from a low-cost uav imagery as tools for monitoring post-fire forest recovery. *Drones (Basel), 3*(1), 6. doi:10.3390/drones3010006

Larson, A. J., & Franklin, J. F. (2005). Patterns of conifer tree regeneration following an autumn wildfire event in the western oregon cascade range, USA. *Forest Ecology and Management, 218*(1-3), 25-36.

Law, B., Hudiburg, T. W., Berner, L. T., Kent, J. J., Buotte, P. C., Harmon, M. E., & Oregon State Univ, C. O. R. (2018). Land use strategies to mitigate climate change in carbon dense temperate forests. *Proceedings of the National Academy of Sciences of the United States of America, 115*(14), 3663-3668. doi:10.1073/pnas.1720064115

Lim, K., Treitz, P., Wulder, M., St-Onge, B., & Flood, M. (2003). LiDAR remote sensing of forest structure. *Progress in physical geography, 27*(1), 88-106. doi:10.1191/0309133303pp360ra

Linder, W. (2006). *Digital photogrammetry : A practical course*. Springer Berlin / Heidelberg.

Lobell, D. B., & Asner, G. P. (2002). Moisture effects on soil reflectance. *Soil Science Society of America journal, 66*(3), 722-727. doi:10.2136/sssaj2002.0722

McCaffrey, D., & Hopkinson, C. (2020). Repeat oblique photography shows terrain and fire-exposure controls on century-scale canopy cover change in the alpine treeline ecotone. *Remote sensing (Basel, Switzerland), 12*(10), 1569. doi:10.3390/rs12101569

McCarley, T. R., Hudak, A. T., Sparks, A. M., Vaillant, N. M., Meddens, A. J. H., Trader, L., . . . Boschetti, L. (2020). Estimating wildfire fuel consumption with multitemporal airborne laser scanning data and demonstrating linkage with modis-derived fire radiative energy. *Remote Sensing of Environment, 251*, 112114. doi:10.1016/j.rse.2020.112114

McKenzie, D. A., & Tinker, D. B. (2012). Fire-induced shifts in overstory tree species composition and associated understory plant composition in glacier national park, montana. *Plant ecology, 213*(2), 207-224. doi:10.1007/s11258-011-0017-x

Meng, R., Dennison, P. E., Huang, C., Moritz, M. A., & D'Antonio, C. (2015). Effects of fire severity and post-fire climate on short-term vegetation recovery of mixed-conifer and red fir forests in the sierra nevada mountains of california. *Remote Sensing of Environment, 171*, 311-325.

Meng, R., Wu, J., Zhao, F., Cook, B. D., Hanavan, R. P., & Serbin, S. P. (2018). Measuring short-term post-fire forest recovery across a burn severity gradient in a mixed pine-oak forest using multi-sensor remote sensing techniques. *Remote Sensing of Environment, 210*, 282-296.

Minore, D. (1971) Shade Benefits Douglas-Fire in Southwestern Oregon Cutover Area. *Tree Planters' Notes,* 22(1).

Moser, B., Temperli, C., Schneiter, G., & Wohlgemuth, T. (2010). Potential shift in tree species composition after interaction of fire and drought in the central alps. *European Journal of Forest Research*, *129*(4), 625-633.

Naesset, E. (1997). Determination of mean tree height of forest stands using airborne laser scanner data. *ISPRS Journal of Photogrammetry and Remote Sensing, 52*(2), 49-56. doi:10.1016/S0924-2716(97)83000-6

Naveed, F., Hu, B., Wang, J., & Hall, G. B. (2019). Individual tree crown delineation using multispectral LiDAR data. *Sensors, 19*(24), 5421.

Nijland, W., de Jong, R., de Jong, S. M., Wulder, M. A., Bater, C. W., & Coops, N. C. (2014). Monitoring plant condition and phenology using infrared sensitive consumer grade digital cameras. *Agricultural and forest meteorology, 184,* 98-106. doi:10.1016/j.agrformet.2013.09.007

Nuijten, R., Coops, N., Goodbody, T., & Pelletier, G. (2019). Examining the multi-seasonal consistency of individual tree segmentation on deciduous stands using digital aerial photogrammetry (dap) and unmanned aerial systems (uas). *Remote sensing (Basel, Switzerland), 11*(7), 739. doi:10.3390/rs11070739

Odum, E. P. (1969). The strategy of ecosystem development. In *The ecological design and planning reader* (pp. 203-216): Springer.

Okhrimenko, M., Coburn, C., & Hopkinson, C. (2019). Multi-spectral LiDAR: Radiometric calibration, canopy spectral reflectance, and vegetation vertical svi profiles. *Remote sensing (Basel, Switzerland), 11*(13), 1556. doi:10.3390/rs11131556

Okhrimenko, M., & Hopkinson, C. (2019). Investigating the consistency of uncalibrated multispectral LiDAR vegetation indices at different altitudes. *Remote sensing (Basel, Switzerland), 11*(13), 1531. doi:10.3390/rs11131531

Parks Canada. (2018a). Green scene. Retrieved from https://www.pc.gc.ca/en/pn-np/ab/waterton/nature/environment/verdure-green

Parks Canada. (2018b). Climate. Retrieved from https://www.pc.gc.ca/en/pn-np/ab/waterton/nature/environment/climat-climate

Parks Canada. (2019). Fire. Retrieved from https://www.pc.gc.ca/en/pn-np/ab/waterton/nature/environment/feu-fire

Parks Canada. (2021). Fire on the mountain. Retrieved from https://www.pc.gc.ca/en/pn-np/ab/waterton/nature/environment/feu-fire/montagne-mountain

Pedro, M. S., Rammer, W., & Seidl, R. (2015). Tree species diversity mitigates disturbance impacts on the forest carbon cycle. *Oecologia, 177*(3), 619-630.

Potter, C., Klooster, S., Crabtree, R., Huang, S., Gross, P., & Genovese, V. (2011). Carbon fluxes in ecosystems of yellowstone national park predicted from remote sensing data and simulation modeling. *Carbon Balance and management, 6*(1), 3.

Reid, D. E., Lieffers, V. J., & Silins, U. (2004). Growth and crown efficiency of height repressed lodgepole pine; are suppressed trees more efficient? *Trees, 18*(4), 390-398.

Rodman, K. C., Veblen, T. T., Battaglia, M. A., Chambers, M. E., Fornwalt, P. J., Holden, Z. A., . . . Rother, M. T. (2020). A changing climate is snuffing out post-fire recovery in montane forests. *Global Ecology and Biogeography, 29*(11), 2039-2051.

Rother, M. T. (2015). Conifer regeneration after wildfire in low-elevation forests of the colorado front range: Implications of a warmer, drier climate.

Rother, M. T., & Veblen, T. T. (2016). Limited conifer regeneration following wildfires in dry ponderosa pine forests of the colorado front range. *Ecosphere, 7*(12), e01594. doi:ARTN e0159410.1002/ecs2.1594

Rother, M. T., & Veblen, T. T. (2017). Climate drives episodic conifer establishment after fire in dry ponderosa pine forests of the colorado front range, USA. *Forests, 8*(5), 159.

Rother, M. T., Veblen, T. T., & Furman, L. G. (2015). A field experiment informs expected patterns of conifer regeneration after disturbance under changing climate conditions. *Canadian Journal of Forest Research, 45*(11), 1607-1616. doi:10.1139/cjfr-2015-0033

Seidl, R., Spies, T.A., Rammer, W., Steel, A.E., Pabst, R.J., Olsen, K. (2012) Multi-scale Drivers of Spatial Variation in Old-Growth Forest Carbon Density Disentangled with LiDAR and an Individual-Based Landscape Model. *Ecosystems* 15, 1321–1335 (2012). https://doi.org/10.1007/s10021-012-9587-2

Shellito, B.A. (2023). *Introduction to Geospatial Technologies* (Sixth edition). Macmillan Learning.

Sonnentag, O., Hufkens, K., Teshera-Sterne, C., Young, A. M., Friedl, M., Braswell, B. H., . . . Richardson, A. D. (2012). Digital repeat photography for phenological research in forest ecosystems. *Agricultural and forest meteorology, 152*(1), 159-177. doi:10.1016/j.agrformet.2011.09.009

Steel, Z. L., Koontz, M. J., & Safford, H. D. (2018). The changing landscape of wildfire: Burn pattern trends and implications for california's yellow pine and mixed conifer forests. *Landscape ecology, 33*(7), 1159-1176.

Storey, E.A., Stow, D.A., O'Leary. (2016). Assessing postfire recovery of chamise chaparral using multi-temporal spectral vegetation index trajectories derived from Landsat imagery. *Remote Sensing of Environment,* doi: 10.1016/j.rse.2016.05.018.

Swetnam, T. L., Brooks, P. D., Barnard, H. R., Harpold, A. A., & Gallo, E. L. (2017). Topographically driven differences in energy and water constrain climatic control on forest carbon sequestration. *Ecosphere, 8*(4), e01797.

Tautenhahn, S., Lichstein, J. W., Jung, M., Kattge, J., Bohlman, S. A., Heilmeier, H., . . . Wirth, C. (2016). Dispersal limitation drives successional pathways in central siberian forests under current and intensified fire regimes. *Global Change Biology, 22*(6), 2178-2197. doi:10.1111/gcb.13181

Tepley, A. J., Swanson, F. J., & Spies, T. A. (2014). Post-fire tree establishment and early cohort development in conifer forests of the western cascades of oregon, USA. *Ecosphere, 5*(7), 1-23.

Tepley, A. J., Thompson, J. R., Epstein, H. E., & Anderson-Teixeira, K. J. (2017). Vulnerability to forest loss through altered postfire recovery dynamics in a warming climate in the klamath mountains. *Glob Chang Biol, 23*(10), 4117-4132. doi:10.1111/gcb.13704

Tepley, A. J., & Veblen, T. T. (2015). Spatiotemporal fire dynamics in mixed-conifer and aspen forests in the san juan mountains of southwestern colorado, USA. *Ecological Monographs, 85*(4), 583-603.

Turner, M. G., Romme, W. H., Gardner, R. H., & Hargrove, W. W. (1997). Effects of fire size and pattern on early succession in yellowstone national park. *Ecological Monographs, 67*(4), 411-433. doi:10.1890/0012-9615(1997)067[0411:EOFSAP]2.0.CO;2

Turner, M. G., Tinker, D. B., Romme, W. H., Kashian, D. M., & Litton, C. M. (2004). Landscape patterns of sapling density, leaf area, and aboveground net primary production in postfire lodgepole pine forests, yellowstone national park (USA). *Ecosystems, 7*(7), 751.

Turner, M. G., Whitby, T., Tinker, D., & Romme, W. (2016). Twenty-four years after the yellowstone fires: Are postfire lodgepole pine stands converging in structure and function? *Ecology, 97*(5), 1260-1273.

Urza, A. K., & Sibold, J. S. (2017). Climate and seed availability initiate alternate post-fire trajectories in a lower subalpine forest. *Journal of vegetation science, 28*(1), 43-56.

Westerling, A. L. (2016). Increasing western us forest wildfire activity: Sensitivity to changes in the timing of spring. *Philosophical Transactions of the Royal Society B: Biological Sciences, 371*(1696), 20150178.

Zhao FR., Meng R., Huang C., Zhao M., Zhao FA, Gong P., Yu L., Zhu Z., (2016). Long-Term Post-Disturbance Forest Recovery in the Greater Yellowstone Ecosystem Analyzed Using Landsat Time Series Stack. *Remote Sensing*. 2016; 8(11):898. https://doi.org/10.3390/rs8110898

Zehetgruber, B., Kobler, J., Dirnböck, T., Jandl, R., Seidl, R., & Schindlbacher, A. (2017). Intensive ground vegetation growth mitigates the carbon loss after forest disturbance. *Plant and soil, 420*(1-2), 239-252.